

JYX



This is a self-archived version of an original article. This version may differ from the original in pagination and typographic details.

Author(s): Huang, Jun; Domínguez-Flores, Fabiola; Melander, Marko

Title: Variants of Surface Charges and Capacitances in Electrocatalysis : Insights from Density-Potential Functional Theory Embedded with an Implicit Chemisorption Model

Year: 2024

Version: Published version

Copyright: © Authors 2024

Rights: CC BY 4.0

Rights url: <https://creativecommons.org/licenses/by/4.0/>

Please cite the original version:

Huang, J., Domínguez-Flores, F., & Melander, M. (2024). Variants of Surface Charges and Capacitances in Electrocatalysis : Insights from Density-Potential Functional Theory Embedded with an Implicit Chemisorption Model. *PRX Energy*, 3, Article 043008.
<https://doi.org/10.1103/prxenergy.3.043008>

Variants of Surface Charges and Capacitances in Electrocatalysis: Insights from Density-Potential Functional Theory Embedded with an Implicit Chemisorption Model


Jun Huang^{1,2,3,*}, Fabiola Domínguez-Flores^{4,†}, and Marko Melander^{4,†}

¹*Institute of Energy Technologies, IET-3: Theory and Computation of Energy Materials, Forschungszentrum Jülich GmbH, 52425 Jülich, Germany*

²*Theory of Electrocatalytic Interfaces, Faculty of Georesources and Materials Engineering, RWTH Aachen University, Aachen 52062, Germany*

³*Jülich Aachen Research Alliance JARA Energy & Center for Simulation and Data Science (CSD), 52425 Jülich, Germany*

⁴*Department of Chemistry, Nanoscience Center, University of Jyväskylä, P.O. Box 35 (YN), FI-40014, Jyväskylä, Finland*

 (Received 13 May 2024; revised 28 August 2024; accepted 23 October 2024; published 15 November 2024)

Prevalent electrolyte effects across a wide range of electrocatalytic reactions underscore the general importance of the local reaction conditions in the electrical double layer (EDL). Compared to traditional EDLs, the electrocatalytic siblings feature partially charged chemisorbates that could blur our long-held views of surface charge densities and differential capacitances—two interrelated quantities shaping the crucial local reaction conditions. Herein, five variants of surface charge density and three variants of differential capacitance in the presence of chemisorbates are defined and compared. A semiclassical model of electrocatalytic EDLs is developed for a quantitative analysis of the differences and interrelationships between these variants of surface charge densities and differential capacitances. It is revealed that the potential- and concentration-dependent net charge on these chemisorbates dramatically changes the surface charge densities and differential capacitances. Specifically, the free surface charge density could decrease as the electrode potential becomes more positive, implying that the *corresponding differential capacitance is negative*. The relationship between the free and total surface charge densities is analyzed with aid of the concept of electrosorption valency. By linking the electrosorption valency with the differential capacitance in the absence of chemisorbates, we explain the potential and concentration dependence of the former. The conceptual analysis presented in this work has important implications for experimental characterization and first-principles-based atomistic simulations of electrocatalysis and EDL effects. Particularly, we disclose a hidden yet potentially crucial disadvantage of widely employed atomistic simulation models that fix the coverage of chemisorbates. Proposing the self-consistent implicit model as an expedient remedy for this disadvantage, this work contributes to more realistic modeling of electrocatalytic EDLs.

DOI: [10.1103/PRXEnergy.3.043008](https://doi.org/10.1103/PRXEnergy.3.043008)

I. INTRODUCTION

Electrocatalytic reactions proceed *via* the adsorption and desorption of chemisorbed intermediates. The thermodynamic state of the chemisorbed intermediates and

the kinetic rate of their adsorption and desorption are determined by both solid and liquid components of the electrode-electrolyte interface, as exemplified by the hydrogen evolution reaction (HER). On one hand, the exchange current density, $J_{0,HER}$, can vary up to 7 orders of magnitude among different metallic electrodes [1–3]. The catalytic trends between different metals have been successfully rationalized using the Sabatier principle [4,5] and modern theories of chemisorption and electrocatalysis [6–9]. On the other hand, $J_{0,HER}$ at Pt(111) is around 20 times higher in 0.05M H₂SO₄ than in 0.1M NaOH [10]. Moreover, $J_{0,HER}$ in alkaline solutions decreases with increasing effective cation size ($Li^+ > Na^+ > K^+ >$

*Contact author: ju.huang@fz-juelich.de

†Contact author: marko.m.melander@jyu.fi

Published by the American Physical Society under the terms of the Creative Commons Attribution 4.0 International license. Further distribution of this work must maintain attribution to the author(s) and the published article's title, journal citation, and DOI.

Cs⁺) at Ir, Pd, Pt electrodes, while the trend is reversed at Cu, Ag, Au electrodes [11,12]. Remarkable electrolyte effects have also been reported for oxygen reduction [13–19], oxygen evolution [20–25], and carbon dioxide reduction [26–29], as well as other electrocatalytic reactions, on various catalysts, underpinning the crucial impact of both the liquid and solid components on electrocatalytic activity and selectivity.

Understanding the origins of these electrolyte effects is a long-standing and classical, yet topical, problem in electrocatalysis, as reflected by a review written by Frumkin in 1959 [30] and recent vigorous research endeavors [31–33]. Recent emphasis has been targeted towards the local reaction conditions within the nanometric electrical double layer (EDL) at the electrode-electrolyte interface [31–37]. Within the theoretical and computational electrocatalysis fields, there is a strong consensus on the need to extend the standard computational hydrogen electrode (CHE) method by incorporating the EDL effects [38–44]. However, it remains unresolved how these effects should be described in an efficient, accurate, and general way; as a result, various approaches from constant-charge to constant-potential schemes have been proposed and are under constant development.

The constant-charge scheme involves complementing the canonical free energy calculated using the CHE method with various electrostatic correction terms, mostly of the form $-C(U - U_0)^2/2$, where C is an effective capacitance, U_0 is the electrode potential corresponding to the canonical DFT slab model, and U is the electrode potential of interest [45–47]. In this sense, the constant-charge scheme adopts the Helmholtz model for the EDL, describing it as a capacitor with a constant capacitance in the potential range between U and U_0 [48,49]. The constant-charge scheme is handy and widely used, since only *a posteriori* correction of EDL effects is required, without resorting to an explicit treatment of the EDL. However, these models need a good model of C . Most often, C is treated as a constant, which cannot be considered a generally valid approximation [47].

The constant-potential scheme entails grand-canonical free energy calculations [38,40,41,43]. A fully grand-canonical scheme should allow the electron number (N_e); the coverage of chemisorbates (θ_i); and the numbers of cations (N_c), anions (N_a), and solvent molecules (N_s) to vary as functions of the electrochemical potentials of these components [50]. Since genuine fully grand-canonical calculations are prohibitively expensive and need nontrivial methodological efforts beyond the current models, various approximations have been introduced in practical applications, including an implicit treatment of the electrolyte solution and a reduced number of grand-canonical variables [47,51]. Crucially, available implicit solvent models for DFT simulations cannot treat chemisorption or covalent bonding; instead, they are restricted to only “outer-Helmholtz layer” effects dictated mainly by electrostatic

interactions [51]. Therefore, current constant-potential calculations tacitly assume a fixed coverage of chemisorbates and should, hence, be referred to as *electronically* grand-canonical [43] or *semi*-grand-canonical simulations [47].

While the constant-charge and constant-potential simulations are thermodynamically equivalent and related to each other *via* a Legendre transformation [47,52–54], the inability to treat chemisorption implicitly impacts them differently. Constant-potential calculations require a good computational model of the capacitance *a priori*. By contrast, constant-charge calculations can correct for the capacitance *a posteriori* using even experimental capacitance data. Therefore, provided with adequate knowledge about the differential capacitance of the EDL, it is possible to calculate the constant-potential free energy from its constant-charge counterpart [47,52–54]. While it is claimed that constant-charge calculations are more immune to inaccuracies and omissions in the computed capacitance, it should be emphasized that it is not any easier to obtain accurate differential capacitances than to self-consistently carry out constant-potential calculations directly. For instance, it has been shown in the example of the acidic Volmer step on Au(111) that the constant-charge scheme with a constant-capacitor approximation agrees quantitatively with the *electronically* grand-canonical scheme [54]. However, the grand-canonical calculations were performed by fixing the chemisorbate coverage in a single *electronically* grand-canonical calculation. Importantly, changes in coverage during the reaction, as required by a *fully* grand-canonical calculation of reaction kinetics [55], have not been addressed.

The consequences of constraining the chemisorbate coverage have, however, barely been discussed. What consequences does the constrained chemisorbate coverage have on the grand-canonical free energies? This question is transformed to understand the influence of chemisorption and potential-dependent chemisorbate coverage on the differential capacitance that bridges canonical and grand-canonical free energies. As we show below, there are at least three capacitances in the presence of chemisorbates. It is not well agreed upon in the literature which one should be used in the conversion between the electrode charge and the electrode potential. Moreover, we show that chemisorption changes not only the magnitude of the capacitance, as tacitly assumed previously, but also *the sign of the differential capacitance*. Our results imply that *electronically* grand-canonical methods with constrained chemisorbate coverages cannot describe this essential characteristic of electrocatalytic EDLs. Likewise, the fully self-consistent implementation of constant-charge calculations should consider the impact of the chemisorption-induced changes in the differential capacitance. As a step forward towards fully self-consistent simulations of electrocatalytic EDLs, we propose a practical way to include

variable chemisorbate coverages in *electronically* grand-canonical simulations through an advanced semiclassical implicit electrolyte model.

II. CONCEPTS

As discussed in Sec. I, both constant-charge and constant-potential simulations of EDL effects require knowledge of the differential interfacial capacitance (C), which is defined as the electrode potential derivative of the surface charge density. In what follows, we begin by laying out a few basic concepts of electrocatalytic EDLs. Specifically, we define several types of differential capacitances and surface charge densities for electrocatalytic EDLs with chemisorbates. Then, we develop a semiclassical model of electrocatalytic EDLs to allow for a quantitative discussion on the differences and relationships between these variants. Afterwards, the semiclassical model is applied to understand the influence of chemisorption on the differential capacitances and surface charge densities. In the end, we relate the insights learned from the semiclassical model to experimental characterization of electrocatalytic EDLs and DFT-based models. For the latter aspect, the emphasis is put on understanding the consequence of the fixed chemisorbate coverage in *electronically* grand-canonical models and their future improvements towards a *fully* grand-canonical model of EDLs.

A. Surface charge densities

An atomistic simulation of an EDL yields the volumetric charge density (ρ), not the surface charge density [56]. Surface charge density is obtained by integrating the volumetric charge density along a particular line, most often the line perpendicular to the electrode surface.

$$\sigma = \int_{z_s}^{z_e} (\rho_n + \rho_e) dz \quad (1)$$

where ρ_n is the volumetric charge density of nuclei, and ρ_e is that of electrons which is negative. It needs to be noted that the selection of the starting and ending points of the line, z_s and z_e , respectively, make the quantification of σ ambiguous. This is true even for ideally polarizable EDLs, e.g., that of the Ag(111)-aqueous KPF₆ solution interface, because the overlap between the electron tail of the metal and the electron cloud of water molecules makes it impossible to rigorously define a surface charge density, σ . Nevertheless, the electroneutrality condition implies that

$$\sigma = -\frac{(N_c - N_a)|e|}{A_{\text{surface}}} \quad (2)$$

where N_c and N_a are the number of K⁺ and PF₆⁻ in the electrolyte solution, respectively; $|e|$ is the elementary charge; and A_{surface} is the geometrical area of the metal surface. For

ideally polarizable EDLs, the states at the Fermi level are fully localized on the metal side, and excess electrons are added to or removed from the metal alone, which can be quantified by the projected density of states on the metal states.

In constant-charge DFT simulations of the EDL, Eq. (2) implies that one can tune σ by varying the type and number of ions in the electrolyte solution [57–59]. The corresponding electrode potential is then obtained from the self-consistently computed Fermi level or the inner potential of the system. In this scheme, the potential of zero charge (PZC) usually corresponds to metal-water interfaces. Rigorously speaking, this potential is the potential of zero ions (PZI) because there are no electrolyte ions in the liquid phase. On the contrary, at the PZC an equal number of cations and anions exist in the EDL. The PZC and PZI are not necessarily identical since the presence of cations and anions in the EDL at the PZC may change the configuration of interfacial water molecules, and thereby impact both the Fermi level of the system and entropy.

Though σ defined in Eq. (2) is unambiguous, it does not offer a clear connection with σ from Eq. (1) due to the spatial overlap of metal electrons and electrons of electrolyte components. Given that electrons are indistinguishable particles, and that charge partition cannot be defined uniquely, one cannot assign the electrolyte, solvent, or electrodes charge without extrathermodynamic assumptions. It is very plausible that one cannot use Eq. (1) to unambiguously obtain the same σ expressed in Eq. (2), no matter how we choose z_s and z_e . Therefore, Eq. (2) is a pragmatic definition based on a modelistic picture.

Compared to “simple” EDLs without chemisorption, the EDLs encountered in electrocatalysis are even more complex, as they feature chemisorbed ions and solvent molecules [31,60,61]. In a modelistic picture, these chemisorbates in the inner Helmholtz plane (IHP) bear a net charge and/or a dipole moment. The charge on chemisorbed ions is different from that of the same ions in the bulk solution, due to the formation of chemical bonds between these ions and the electrode. This has been revealed in the theory of chemisorption [6–9] and quantum chemical simulations [62]. Moreover, the chemisorbed ions do not need to carry an integer charge but are typically partially charged. This fact further complicates the definition and calculation of surface charge densities. As a result, at least five different types of surface charge densities can be defined, as summarized in Fig. 1: the total surface charge density (σ_{tot}), the free surface charge density (σ_{free}), the metal surface charge density (σ_M), the total and net charge density of chemisorbates ($\sigma_{\text{ad,tot}}$, $\sigma_{\text{ad,net}}$). All these quantities are related but only some are measurable while others are modelistic quantities. We will explore their relationships and characteristics.

σ_{tot} is a measurable quantity, as it corresponds to the total amount of electrons flowing through the external

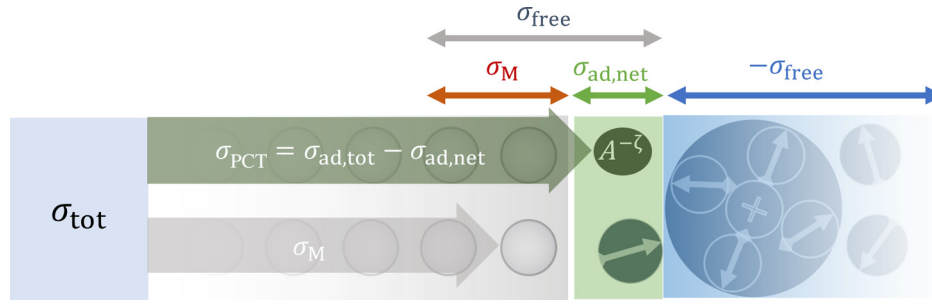


FIG. 1. Surface charge densities of electrocatalytic EDLs. Total charge density, σ_{tot} , measures the total amount of electrons flowing through the external circuit when the electrode is subject to a given potential. Metal charge density, σ_{M} , is a modelistic concept, describing the surface charge density within the metal region, of which the outer boundary is indefinite in the presence of chemisorbates. Total and net charge density of partially charged chemisorbates are $\sigma_{\text{ad,tot}}$ and $\sigma_{\text{ad,net}}$, respectively, and their difference is the amount of charge transferred between the metal and the chemisorbed ion, namely, the charge involved in the partial charge transfer process, denoted σ_{PCT} . Total charge density σ_{tot} is divided into σ_{PCT} , charging the chemisorbates, and σ_{M} , charging the metal. Amount of charge stored in the diffuse layer stretching from the outer Helmholtz plane to the bulk solution is the negative of the free charge density, σ_{free} . Since the overall EDL is electroneutral, σ_{free} is the sum of σ_{M} and $\sigma_{\text{ad,net}}$, which establishes a rigid dichotomy between the metal and the chemisorbates.

circuit upon changing the electrode potential. It also bears thermodynamic significance. The electrocapillary equation links it with the interfacial tension and electrode potential: $\sigma_{\text{tot}} = (\partial\gamma/\partial E)_{\tilde{\mu}_i}$, with γ being the interfacial tension, E is the electrode potential, and $\tilde{\mu}_i$ is the electrochemical potentials of the constituents of the electrolyte solution [63,64]. σ_{tot} was often denoted as σ_{M} in earlier references, e.g., Ref. [65]. Lorenz and Salié thus termed σ_{tot} the thermodynamic charge density [66], while Frumkin and Petrii coined the name total charge density [67]. In the presence of chemisorption, σ_{tot} contains contributions from EDL charging or discharging, chemisorbate adsorption or desorption, and the nontrivial coupling of these processes.

The potential-dependent changes in σ_{tot} can be understood using a simple *gedanken* experiment of a single anion chemisorption at constant potential. Let us first freeze all other components of the EDL and move a monovalent anion from the bulk solution to the IHP. No matter how the extra valence electron is shared between the electrode and the anion, an electron must flow out of the electrode to ensure overall electroneutrality. However, the presence of this partially charged chemisorbed anion brings up an extra potential drop between the metal surface and the IHP. To retain the electrode potential, this potential drop must be compensated for and screened by accumulation of counterions in the diffuse layer. Therefore, a certain number of cations move into the diffuse layer, rendering an equal number of electrons flowing back into the electrode. In sum, the change in σ_{tot} is less than one electron upon chemisorption of a monovalent anion.

Extending from this example, we consider a general case involving multiple types of chemisorbed ions with surface coverages $\theta_i = N_i/N_{\text{M}}$, with N_{M} being the areal density of metal atoms and N_i that of adsorbates i . We denote the partial charges of these chemisorbed ions as q_i and their

corresponding bulk charges q_i^{b} . The total charge density of chemisorbates $\sigma_{\text{ad,tot}}$ is

$$\sigma_{\text{ad,tot}} = \sum_i \theta_i N_{\text{M}} q_i^{\text{b}}, \quad (3)$$

and the net charge density of chemisorbates, $\sigma_{\text{ad,net}}$, is

$$\sigma_{\text{ad,net}} = \sum_i \theta_i N_{\text{M}} q_i. \quad (4)$$

We note that $|\sigma_{\text{ad,net}}| \leq |\sigma_{\text{ad,tot}}|$.

One can also use Frumkin's definition of free surface charge, σ_{free} [67], where "free" means that the addition (removal) of these ions does not involve the formation (cleavage) of chemical bonds. Put in an equivalent way, the addition (removal) of these ions is purely of electrostatic origin. Since the outer Helmholtz plane (OHP) is the closest plane that nonspecifically adsorbed ions can approach the electrode surface, a pragmatic definition of σ_{free} is [56]

$$\sigma_{\text{free}} = - \int_{z_{\text{OHP}}}^{z_{\infty}} \left(\sum_i n_i q_i^{\text{b}} \right) dz, \quad (5)$$

where z_{OHP} denotes the OHP, z_{∞} is the bulk solution, and n_i is the number density of ions.

As in the example of anion chemisorption, the total surface charge density is then a sum of the negative of the total adsorbate charge density and the surface free charge density:

$$\sigma_{\text{tot}} = -\sigma_{\text{ad,tot}} + \sigma_{\text{free}}, \quad (6)$$

where the negative sign before $\sigma_{\text{ad,tot}}$ means that the electrode charge tends to counterbalance the charge carried

by the chemisorbates. In some cases, the negative sign is omitted when $\sigma_{\text{ad,tot}}$ is defined with respect to the electrode charge.

It is also important to note that σ_{free} and $\sigma_{\text{ad,tot}}$ are coupled. The immediate influence of this coupling is that the chemisorption of a monovalent anion results in a fraction of an elementary charge flowing in the external circuit. This leads to the concept of electrosorption valency, l [64,66], which is formally defined in Eq. (9).

Because σ_{tot} is measurable, Eq. (6) indicates that σ_{free} is known if θ_i can be measured, e.g., using optical spectroscopy approaches [68–70]. However, as σ_{free} is much smaller than both σ_{tot} and $\sigma_{\text{ad,tot}}$, the accuracy of calculating the difference between two large numbers is a perplexing issue.

It is important to note that the relationship $\sigma_{\text{M}} = \sigma_{\text{free}}$ does not hold for the case with chemisorption due to the presence of nonzero adsorbate charge, $\sigma_{\text{ad,net}}$. Instead, we have

$$\sigma_{\text{M}} + \sigma_{\text{ad,net}} = \sigma_{\text{free}}, \quad (7)$$

as illustrated in Fig. 1.

Substituting Eq. (7) into Eq. (6) leads to

$$\sigma_{\text{tot}} = -\sigma_{\text{PCT}} + \sigma_{\text{M}}, \quad (8)$$

where $\sigma_{\text{PCT}} = (\sigma_{\text{ad,tot}} - \sigma_{\text{ad,net}})$ is the partial charge transferred from chemisorbates to the electrode.

We wish to emphasize that these formal definitions of surface charge variants are not solely driven by academic curiosity; rather, they play a crucial role in delineating modelistic quantities from measurable quantities, thus fundamentally shaping the modeling and understanding of capacitance and, consequently, EDL effects in electrocatalysis.

B. Electrosorption valency

The electrosorption valency, l_i , is a key quantity in understanding the influence of chemisorption on the differential capacitances, as it measures how the total charge density depends on the surface coverage of a given species [64,66]:

$$l_i = \frac{-1}{N_{\text{M}}} \left(\frac{\partial \sigma_{\text{tot}}}{\partial \theta_i} \right)_{E, \theta_j \neq i}. \quad (9)$$

The electrosorption valency quantifies the negative of the total charge flowing through the external circuit upon chemisorption of an ion i at constant electrode potential and coverages of other chemisorbates. l_i is different from q_i^{b} since σ_{free} varies during the chemisorption process, as seen in the *gedanken* experiment.

For the usual case with only one type of chemisorbed ion, the electrosorption valency can be reformulated as

$$l_i = -q_i^{\text{b}} \left(\frac{\partial \sigma_{\text{tot}}}{\partial \sigma_{\text{ad,tot}}} \right)_E. \quad (10)$$

Combining Eqs. (6) and (10) leads to

$$l_i = q_i^{\text{b}} - q_i^{\text{b}} \left(\frac{\partial \sigma_{\text{free}}}{\partial \sigma_{\text{ad,tot}}} \right)_E. \quad (11)$$

In summary, l_i reflects the strength of the coupling between σ_{free} and $\sigma_{\text{ad,tot}}$ at constant potential. If σ_{free} and $\sigma_{\text{ad,tot}}$ are decoupled, we retrieve the trivial result, $l_i = q_i^{\text{b}}$.

C. Differential capacitances

The charge density variants lead to corresponding differential capacitance variants defined as

$$C(E) = \left(\frac{\partial \sigma}{\partial E} \right)_{\tilde{\mu}_i}, \quad (12)$$

where we highlight that the capacitance depends on the electrode potential, E , and that the electrochemical potentials, $\tilde{\mu}_i$, are kept constant. According to Eq. (6), the relationship between the total capacitance, $C_{\text{tot}} = \partial \sigma_{\text{tot}} / \partial E$; the double layer capacitance, $C_{\text{DL}} = \partial \sigma_{\text{free}} / \partial E$; and the pseudocapacitance of chemisorption coined by Conway and Gileadi [71], $C_{\text{ad}} = -(\partial \sigma_{\text{ad,tot}} / \partial E)$, is obtained as

$$C_{\text{tot}} = C_{\text{ad}} + C_{\text{DL}}. \quad (13)$$

Inherited from the magnitude difference between $\sigma_{\text{ad,tot}}$ and σ_{free} , C_{ad} is usually much larger than C_{DL} . Therefore, C_{tot} is usually dominated by C_{ad} in the presence of chemisorption, see examples by Refs. [61,72]. Note that C_{ad} and C_{DL} are not independent; instead, C_{DL} is influenced by the adsorbates. Usually, the charging and discharging of the diffuse layer is much faster than the adsorption and desorption of chemisorbates, which allows the separation of C_{ad} and C_{DL} based on the difference of their time constants using, e.g., electrochemical impedance spectroscopy (EIS) [73–77]. In this scenario, the differential capacitance measured at a sufficiently high frequency is $C_{\text{DL, HF}}$, with the subscript ‘‘HF’’ denoting high frequency, while that measured at a sufficiently low frequency is the sum of $C_{\text{DL, LF}}$, with the subscript ‘‘LF’’ denoting low frequency, and C_{ad} . It is important to note that $C_{\text{DL, HF}}$ and $C_{\text{DL, LF}}$ are characteristically different due to the influence exerted by C_{ad} ; we come back to this in Sec. V.

III. THEORETICAL METHODS

The key question to answer is how chemisorption changes the EDL properties. Specifically, we are interested

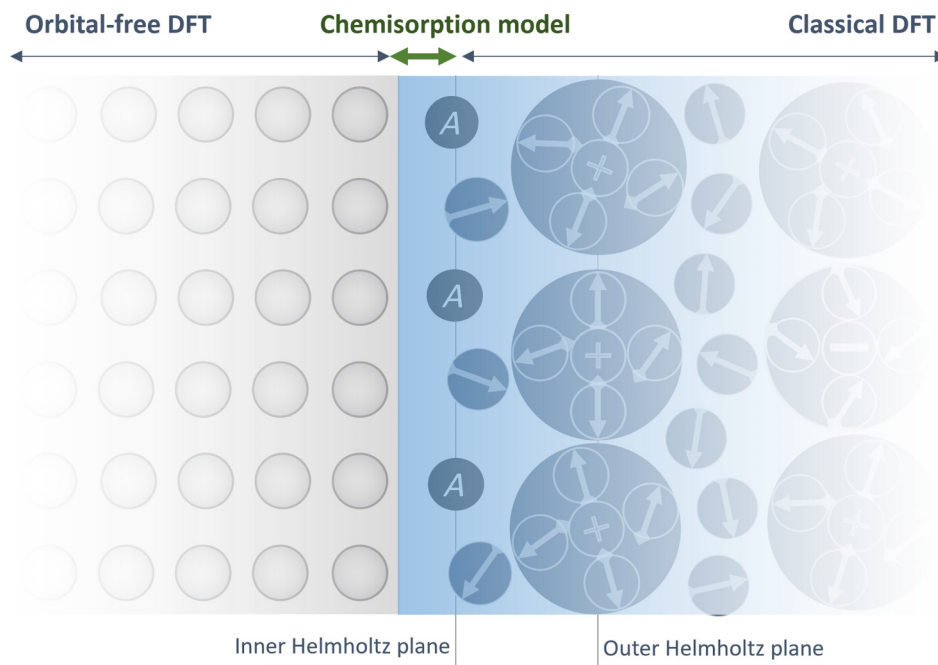


FIG. 2. Schematic diagram of electrocatalytic EDLs with partially charged chemisorbates (intermediates, denoted A) located at the IHP. This work develops a grand-canonical, semiclassical model for electrocatalytic EDLs with an implicit treatment of chemisorption. Specifically, the metal electrons are described using an orbital-free DFT, the electrolyte solution is described using a classical statistical field theory, and metal-solution short-range interactions are described using Morse potentials. Chemisorption of anions is treated using the Anderson-Newns model Hamiltonian approach. The semiclassical model itself does not involve classical modelistic concepts like the IHP and OHP; instead, it describes the whole EDL with continuous density and potential profiles.

in the influence of chemisorption on σ_{free} and C_{DL} , the coupling between $\sigma_{\text{ad,tot}}$ and σ_{free} , and the coupling between C_{ad} and C_{DL} . To address these questions, we need a method capable of modeling the EDL with chemisorption under constant electrode and electrochemical potential conditions. For this purpose, we extend recent density-potential functional theory (DPFT) from previous models developed for ideally polarizable EDLs to EDLs with chemisorption [78–81].

As illustrated in Fig. 2, the DPFT method combines orbital-free DFT of the metal electrons, thermodynamic statistical classical DFT theory of the liquid solution, and parameterized potential relationships for short-range interactions between the metal and the electrolyte solution. In the absence of chemisorption, the DPFT approach is an orbital-free version of the recently developed constant inner-potential DFT (CIP-DFT) approach [82]. DPFT expresses the grand potential of the EDL as a hybrid explicit functional of the electron density and the electrostatic potential. The variational analysis of the grand potential functional is carried out using the Euler-Lagrange equation, resulting in two coupled partial differential equations in terms of the electron density (n_e) and the electrostatic potential (ϕ). These two controlling equations are solved under constant electrochemical potentials of electrons, electrolyte ions, and solvent conditions, namely,

under typical experimental conditions of constant electrode potential and electrolyte activity. As a result, one obtains self-consistent and continuous profiles of electron density, electrostatic potential, ion density, and solvent density. As the model describes the entire *interphase* [83] from the metal phase to the electrolyte or solution phase, the electrostatic potential and all the densities are calculated for the entire interphase. Properly parameterized short-range interactions between the metal and the electrolyte solution separate the two phases, guaranteeing that ions and solvent molecules do not penetrate the metal.

Currently, the orbital-free DFT description cannot reliably treat chemisorption on metal surfaces [84,85]. Here, we adopt a different strategy and treat chemisorption in an implicit modelistic way. The present implicit chemisorption model can also be combined with common Kohn-Sham DFT implementations in electrocatalysis as an extension of available implicit solvent models. Specifically, we employ the Anderson-Newns model Hamiltonian to describe the hybridization of the ion's valence electron orbital with the metal orbitals (bands) [6–9]. The key result from the implicit chemisorption model is the partial charge of the ion, q_i , which depends on the electrode potential and ion position. Since the resultant q_i enters the Euler-Lagrange equation for the electrostatic equation, the electronic structure, adsorbate charge, and electrostatic

potential, as well as the electrolyte densities, are solved self-consistently and are naturally coupled to each other.

A. DPFT-Chem model

Here, we present a brief review of the key equations of the DPFT and refer interested readers to a detailed derivation in a previous work [79]. To extend the DPFT model to electrosorption problems, we reformulate the DPFT equations for the specific case of an Ag(111) electrode immersed in an electrolyte. Motivated by an experimental study [65], we consider the Ag(111) electrode in $c(1-f)MKPF_6 + cfMKCl$ solution, where c is the total molar concentration of anions and $0 \leq f \leq 1$ is the fraction of the chemisorbing Cl^- anion of the total anion concentration. We denote the Ag cationic cores with the abbreviation “CC,” metal electrons with “e,” solvent with “s,” electrolyte cations with “c,” nonspecifically adsorbed PF_6^- anion with “NA,” and chemically adsorbing Cl^- anion with “CA.” The metal electrode is modeled as a jellium.

The controlling equation for the electron density described with orbital-free DFT at the semilocal level is [75]

$$\bar{\nabla} \bar{\nabla} \bar{n}_e = \frac{20}{3} \bar{n}_e \frac{\omega}{\theta_T \omega - \theta_{XC}} \left(\frac{\partial t_{TF}}{\partial \bar{n}_e} + \frac{\partial u_X^0}{\partial \bar{n}_e} + \frac{\partial u_C^0}{\partial \bar{n}_e} - \frac{(|e|\phi + \bar{\mu}_e)}{e_{a.u.}} \right) + \frac{(\theta_T \omega - \frac{4}{3} \theta_{XC})}{2 \bar{n}_e (\theta_T \omega - \theta_{XC})} (\bar{\nabla} \bar{n}_e)^2, \quad (14)$$

where $\omega = (2/5)\pi^{5/3} 3^{1/3} (\bar{n}_e)^{1/3}$ is a density-dependent coefficient; $\bar{n}_e = n_e(a_0)^3$, using the Bohr radius, a_0 , as the reference length is the dimensionless electron density; $\bar{\nabla} = a_0 \nabla$ is the dimensionless gradient operator; θ_T and

θ_{XC} are the coefficients of the “semilocal” gradient terms in kinetic energy and exchange-correlation energy functional, respectively; t_{TF} is the Thomas-Fermi kinetic energy functional, u_X^0 and u_C^0 are the exchange and correlation energy in the Perdew-Burke-Ernzerhof (PBE) functional, respectively; $|e|$ is the elementary charge; $e_{a.u.} = 27.2$ eV is the reference energy in atomic units; and $\bar{\mu}_e$ is the electrochemical potential of electrons, which corresponds to the electrode potential and is the key control variable in constant-potential experiments. Equation (14) is general and can be applied to both atomic and continuum descriptions of the electrode. Herein, we adopt a jellium description of the electrode.

The controlling equation for the electrostatic potential is [79]

$$-\bar{\nabla} \cdot (\bar{\epsilon}_{OP} \bar{\nabla} \bar{\phi} + \bar{n}_s \bar{p}_s \kappa L_s) = \kappa ((\bar{n}_{CC} - \bar{n}_e) + \bar{n}_c + \bar{n}_{CA} q_{CA} - \bar{n}_{NA}), \quad (15)$$

where $\bar{\phi} = |e|\phi/k_B T$ is the dimensionless electrostatic potential with the Boltzmann constant, k_B , and temperature, T ; $\bar{\epsilon}_{OP}$ is the dimensionless optical permittivity referenced to the permittivity of vacuum, ϵ_0 ; $\bar{n}_l = n_l(a_0)^3$, $l \in \{s, CC, CA, NA\}$ are the dimensionless number densities; $\bar{p}_s = p_s/|e|a$ is the dimensionless dipole moment of the solvent; $\kappa = e_0^2/k_B T \epsilon_0 a_0$ is a unitless number originating from the nondimensionalization process; and $L_s = \coth(\bar{p}_s \bar{E}) - (\bar{p}_s \bar{E})^{-1}$ is the Langevin function with the dimensionless electric field, $\bar{E} = \bar{\nabla} \bar{\phi}$. Recently, Shibata *et al.* extended the DPFT model with an improved description of the electrolyte solution [86].

The number densities are obtained from variational analysis of the grand potential, and are given by

$$\bar{n}_l = \bar{n}_l^b \frac{\Theta_l}{\chi_v + \chi_s \Theta_s + \gamma_{CA} \chi_{CA} \Theta_{CA} + \gamma_{NA} \chi_{NA} \Theta_{NA} + \gamma_c \chi_c \Theta_c}, \quad l \in \{s, c, CA, NA\}, \quad (16)$$

where \bar{n}_l^b is the dimensionless bulk density of species l , $\chi_l = \bar{n}_l^b / \sum_l \bar{n}_l^b$, γ_l is the relative size of species l referenced to that of the solvent molecule, and χ_v is the volume fraction of unoccupied space in the bulk solution.

The Boltzmann factors, Θ_l , are

$$\Theta_l = \exp(-(q_l \bar{\phi} + w_l)), \quad l \in \{c, CA, NA\},$$

$$\Theta_s = \exp\left(-\left(-\ln \frac{\sinh(\bar{p}_s \bar{E})}{\bar{p}_s \bar{E}} + w_s\right)\right), \quad (17)$$

where q_l is 1 for cations ($l = c$), -1 for nonspecifically adsorbing anions ($l = NA$), and fractional for chemisorbed

anions ($l = CA$). The short-range interaction terms, w_l , $l \in \{s, c, CA, NA\}$, are described using Morse potentials [78, 87]:

$$w_l(\vec{r}) = D_l (\exp(-2\beta_l(d(\vec{r}) - b_l)) - 2\exp(-\beta_l(d(\vec{r}) - b_l))), \quad (18)$$

with D_l being the well depth, related to the binding strength; β_l is a coefficient controlling the well width; $d(\vec{r})$ is the distance from a point with coordinate \vec{r} referenced to the metal surface; and b_l the distance to the well bottom. Throughout this paper, we use \vec{r} for coordinates of a point in the space, z for the coordinate in the

direction normal to the surface, and $d(\vec{r})$ for the distance between a point and the metal surface. When \vec{r} is within the metal, $d(\vec{r})$ is negative and $w_l(\vec{r})$ increases exponentially, resulting in a negligible probability of species l in the bulk metal. As the electrode potential varies, the extent of the electron spillover of the metal changes, which ultimately affects the binding strength of the anion on the metal surface. Specifically, the potential-dependent covalent binding strength of the chemisorbed anion, Cl^- in the present work, grows at more positive electrode potential [62,88]. This is approximated through a linear relationship:

$$D_{\text{CA}} = \frac{1}{k_{\text{B}}T}(D_{\text{CA}}^0 + \alpha_{\text{CA}}\tilde{\mu}_e), \quad (19)$$

where the coefficient $\alpha_{\text{CA}} < 0$, and D_{CA}^0 denotes the intercept at $\tilde{\mu}_e = 0$ eV. Note that Eq. (19) does not include the electrostatic interactions, which are described separately through Eq. (17).

The charge of the chemisorbed anion, Cl^- in the present case, is derived from an Anderson-Newns model Hamiltonian treatment detailed in the Supplemental Material [89] (including Refs. [50,90–101]):

$$q_{\text{CA}}(d) = -\frac{1}{2} + \frac{1}{\pi} \arctan\left(\frac{\epsilon_{\text{CA}}}{\Delta}\right), \quad (20)$$

where $\Delta = \Delta^0 \exp(-\kappa_{\Delta}(d - d_{\text{cut}})\theta(d - d_{\text{cut}}))$ is the strength of the electronic metal-anion interaction, which decreases exponentially with the anion moving away from the metal surface; κ_{Δ} is the coefficient determining the exponential decay of Δ ; d is the distance of the anion away from the metal surface; d_{cut} is the cut-off distance; and $\theta(x)$ is the Heaviside function. $\epsilon_{\text{CA}} = -\tilde{\mu}_e + (\epsilon_{\text{CA}}^0 - \Delta_{\epsilon}(1 - \exp(-\kappa_{\epsilon}(d - d_{\text{cut}})\theta(d - d_{\text{cut}}))))$ is the energy of the valence orbital of the anion referenced to the Fermi level of the metal. ϵ_{CA} also changes with the distance d , characterized with a magnitude of $\Delta_{\epsilon} > 0$ and a coefficient of κ_{ϵ} . ϵ_{CA}^0 is the reference value at $d = d_c$. The increase in ϵ_{CA} with decreasing d facilitates transfer of the electron from the anion to the metal.

In summary, the current model has three coupled components, which are to be solved self-consistently. The first component describes the metal phase using orbital-free DFT theory in Eq. (14). Different from standard Kohn-Sham DFT calculations, the electrostatic potential and the electron density are not dual variables here; instead, they have the same status. The second component describes the electrolyte phase using an extended Poisson-Boltzmann equation in Eq. (15). The extension is threefold: solvent orientational polarization of solvent molecules is treated as in dipolar Poisson-Boltzmann theory [102,103]; a unified description of the metal and electrolyte phases removes problems associated with the metal-solution boundary, particularly the image charge problem [104,105]; and the ion

charge is not constant but varies spatially and as a function of the electrode potential due to chemisorption. The partial variable charge of chemisorbed anions is calculated from an Anderson-Newns model Hamiltonian, which is the third component of the current model.

B. Model parameters

The developed model has four groups of parameters. The first group of parameters is related to orbital-free DFT of metal electrons, including θ_{T} calibrated using the experimental PZC and θ_{XC} with recommended values in the PBE functional. The second group of parameters describes the short-range effects between the solvent, electrolyte, and the metal through the Morse potentials, as shown in Eq. (18). The third group of parameters is the structural and electrical properties of electrolyte ions and solvent molecules. The fourth group of parameters is in the Anderson-Newns Hamiltonian describing the chemisorption of anions. The first three groups of parameters are inherited without changes from our previous study on the EDL at the Ag(111)-KPF₆ aqueous solution interface [79]. These parameters were calibrated by benchmarking the model results with experimental differential double layer capacitance profiles for a series of electrolyte concentrations [106]. Additionally, the short-range interaction between Ag(111) and the chloride anion is studied using grand-canonical DFT (GC-DFT) calculations [93]. The details of implementing the GC-DFT calculations are provided in the Supplemental Material [89].

In the previous work [79], the density profiles of electrons, ions, and solvent molecules from the metal phase to the electrolyte phase were obtained for a range of electrochemical potentials. Herein, we disclose the underlying factors determining the density profiles, as these are instrumental to understand the interplay among different components of the model. Equation (16) indicates that \bar{n}_l is determined by the competition between four Boltzmann factors, Θ_l , which are further determined by w_l , $\bar{\phi}$, and $\ln(\sinh(\bar{p}_s \bar{E})/\bar{p}_s \bar{E})$, according to Eq. (17). These terms are displayed in Fig. 3.

Nondimensional short-range interactions between the metal and nonspecifically adsorbing anions (w_{NA}), cations (w_{c}), solvent molecules (w_{s}), and chemisorbed anions (w_{CA}) are illustrated in Fig. 3(a). As expressed in Eq. (18), all w_i profiles transit from zero in the bulk solution to negative values near the metal surface and then to positive values at smaller d . The dip with a value of $-D_l$ is obtained at b_l . Solvent molecules and chemisorbed anions approach the metal surface closer than other species, namely, the values of b_l are smaller for solvent and chemisorbed anions. In addition, the well depth, $-D_l$, is greater for solvent molecules than nonspecifically adsorbing anions and cations.

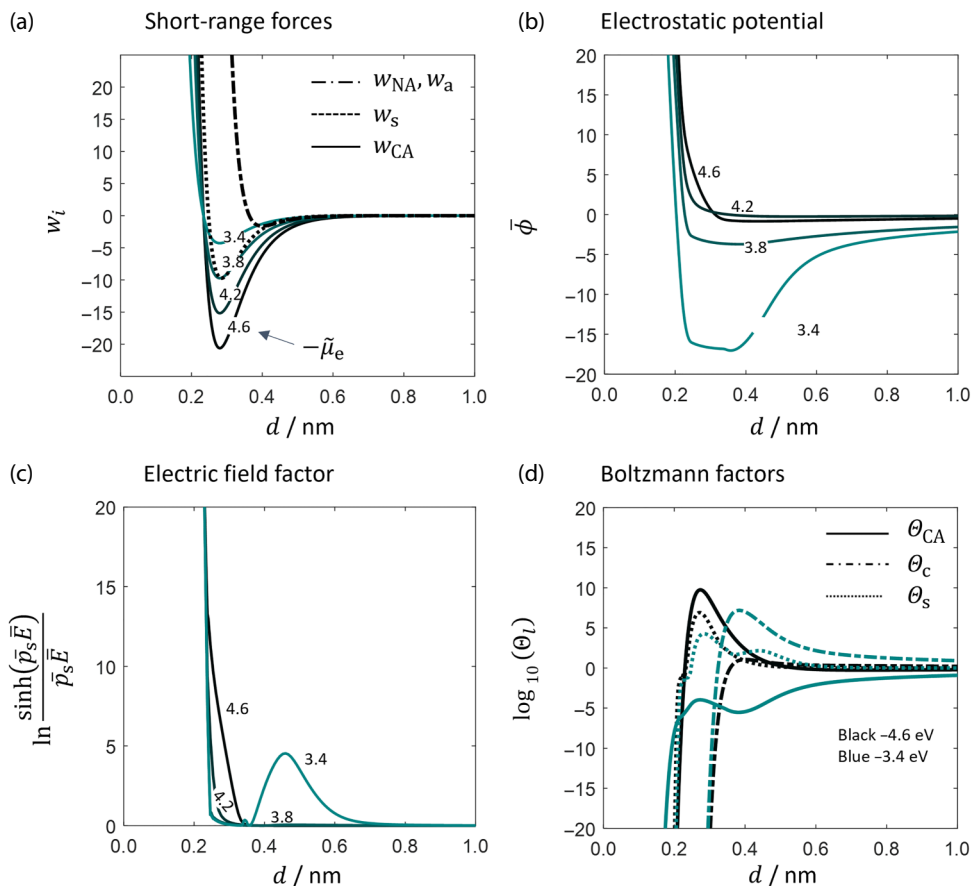


FIG. 3. Decomposition of and comparison between Boltzmann factors. (a) Nondimensional (normalized to $k_B T$) short-range interactions between the metal and nonspecifically adsorbing anions (w_{NA}), cations (w_c), solvent molecules (w_s), and chemisorbed anions (w_{CA}). w_{CA} depends on the electrochemical potential of electrons ($\tilde{\mu}_e$). The x axis denotes the distance to the metal surface, and $d = 0$ denotes the metal edge. (b) Nondimensional (normalized to $k_B T$) electrostatic potential distribution at five electrochemical potentials of electrons. (c) Electric field factor at five electrochemical potentials of electrons. (d) Boltzmann factors of the chemisorbed anions (Θ_{CA}), cations (Θ_c) and solvent molecules (Θ_s) as a function of distance at two electrochemical potentials of electrons.

Figure 3(a) shows that the well is deeper for the chemisorbed anions at more negative $\tilde{\mu}_e$, namely, at more positive electrode potentials. In other words, the binding strength of the chemisorbed anions is stronger at more positive electrode potentials. This trend is supported by our GC-DFT results plotted in Fig. 4(b) for the model system depicted in Fig. 4(a). When comparing the GC-DFT model and the DPFT model, it should be noted that the definition of distance, energy, and electrode potential are different. First, with regard to the distance, d in the GC-DFT model refers to the distance between the outer surfaces of the outermost Ag atom and the chloride atom because the Ag atoms are allowed to relax at each electrode potential and chloride position. Figure 4(a) shows the case of $d = 0$ Å. By contrast, d in the DPFT model refers to the distance between the edge of the jellium, which is half a lattice constant beyond the outer surface of the outermost Ag atom [107], and the center of the chloride atom. Second, the y axes in Figs. 3(a) and 4(b) represent different energies.

Figure 4(b) describes the adsorption grand free energy, denoted $\Delta\Omega$ of Cl^- adsorption, given by Eq. (S15) within the Supplemental Material [89]. Therefore, $\Delta\Omega$ implicitly describes changes in both the short-range covalent interaction energy, w_{CA} , shown in Fig. 3(a), as well as the longer-range electrostatic interactions between the chloride anion, the electrode, and the implicit solvent. A rough estimation indicates that the former short-range forces dominate $\Delta\Omega$. As the electrode potential changes from -0.5 to 0.75 V versus the SHE, $\Delta\Omega$ changes by more than 1 eV, while the mean-field electrostatic energy changes around 0.2 eV, given that the electric potential changes by around 0.4 V [Fig. 3(b)] and the partial charge of the anion is around $-0.5e$ (Fig. 5). Third, the DPFT model uses the electrochemical potential of electrons referenced to vacuum, $\tilde{\mu}_e$, to represent the electrode potential, while the GC-DFT model uses the standard hydrogen electrode (SHE, E_{SHE}) potential scale. These electrode potential references are related, $\tilde{\mu}_e = \tilde{\mu}_e^0 - |e|E_{\text{SHE}}$, with $\tilde{\mu}_e^0$ being the

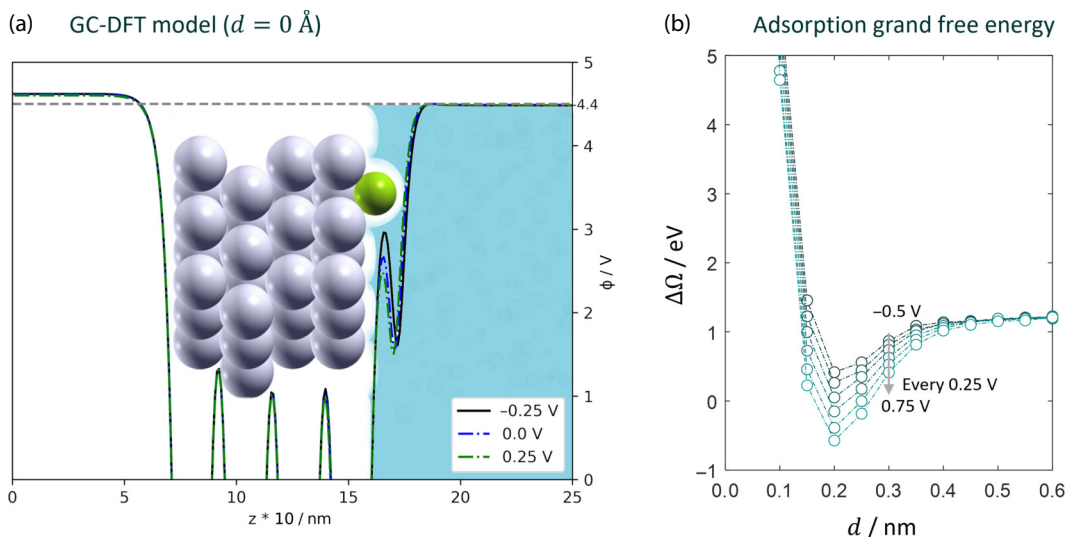


FIG. 4. (a) Schematic of the interface configuration used in the GC-DFT model at $d = 0 \text{ \AA}$. Electrostatic potential profiles at three electrode potentials referenced to the standard hydrogen electrode are shown. Solvated jellium region is shown in blue. (b) Adsorption grand free energy, $\Delta\Omega$, of a chloride anion as a function of its distance from the metal surface, d , and the electrode potential referenced to the standard hydrogen electrode. See a discussion on the definition of d , $\Delta\Omega$, and the electrode potential in the GC-DFT simulation, compared to the DPFT model and experiments, in the text. Data for subplot (b) is tabulated in the Supplemental Material [89].

electrochemical potential of electrons at the SHE referenced to vacuum. While a value of -4.44 eV is often used for $\tilde{\mu}_e^0$, Hörmann and Reuter found that a value of -4.04 eV gave better agreement with experimentally measured adsorption potentials, most likely due to deficiencies in the implicit electrolyte treatment [88,108]. Given these differences, we cannot directly use the GC-DFT results to parametrize the short-range interactions of the DPFT model; instead, the GC-DFT results guide us in properly treating the potential dependency of the short-range force on the chloride anion, as expressed in Eq. (19).

Figure 3(a) shows that short-range potentials are repulsive and the w_i profiles increase exponentially with decreasing d when d is below 0.2 nm . Accordingly, the Boltzmann factors, Θ_i , and the concentrations, n_i , in this region are negligibly small, as shown in Fig. 3(d). This means that electrolyte solution species cannot reside closer to the metal surface due to the strong short-range repulsion. This effectively separates the electrolyte solution from the metal. Note that $\ln(\sinh(\bar{p}_s \bar{E})/\bar{p}_s \bar{E})$ also increases dramatically within $d < 0.2 \text{ nm}$ due to the intrinsic potential drop caused by the electron tail at the metal surface, as shown

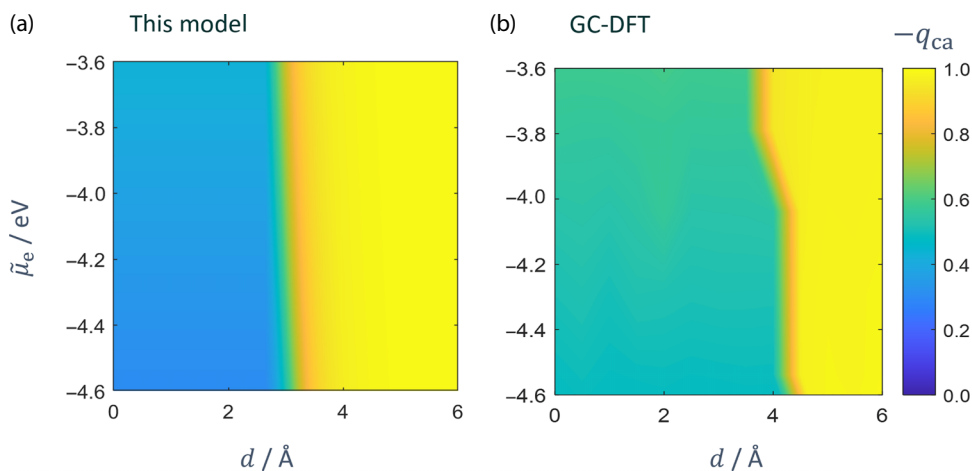


FIG. 5. Partial charge on a chloride anion as a function of its distance from the metal surface, d , and the electrochemical potential of electrons ($\tilde{\mu}_e$). (a),(b) Results obtained from the current model and grand-canonical DFT (GC-DFT) calculations. Electrode potential in the GC-DFT model is rescaled to match the experimental PZC of this system; see a discussion in the text. Model parameters used in this comparison are listed in Table I. Data in subplot (b) is tabulated in the Supplemental Material [89].

TABLE I. Default values of parameters in the Anderson-Newns Hamiltonian of chemisorption, determined by comparing the partial charge profiles from the present model with that from grand-canonical DFT calculations. Together, these parameters allow a reasonable description of the partial charge transfer process. However, the rationality of each single parameter alone is not guaranteed due to the limited data used in model calibration.

Symbol	Meaning	Value
D_{ca}^0	Intercept of the binding strength relationship in Eq. (19) at $\tilde{\mu}_e = 0$ eV	-1.08 eV
α_{ca}	Linear coefficient of the binding strength relationship in Eq. (19)	-0.35
β_{ca}	Coefficient in the Morse potential of chemisorbing anions in Eq. (18)	$0.8/a_0$
b_{ca}	Location of the minimum of the Morse potential of chemisorbing anions in Eq. (18)	2.8 Å
Δ^0	Strength of electronic interactions between the metal and chemisorbing anions	2 eV
κ_Δ	Coefficient determining the exponential decay of electronic interactions	$1/a_0$
d_{cut}	Cutoff distance of the exponential decays	$5a_0$
ϵ_{ca}^0	Reference energy of the valence orbital of chemisorbing anions	-3.2 eV
Δ_ϵ	Overall change of the valence orbital of chemisorbing anions	3 eV
κ_ϵ	Coefficient determining the change rate of the valence orbital of chemisorbing anion	$1/a_0$

in Fig. 3(c). This tends to bring solvent molecules into this region. However, since $w_s \gg \ln(\sinh(\bar{p}_s \bar{E})/\bar{p}_s \bar{E})$, we have $\Theta_s \approx 0$ in this region close to the electrode surface.

In the region of $0.2 \text{ nm} < d < 0.4 \text{ nm}$, either Θ_{CA} or Θ_s is the dominant Boltzmann factor, depending on $\tilde{\mu}_e$, as shown in Fig. 3(d). Cations and nonspecifically adsorbed anions have a negligibly small density in this region because of the distance from the Morse potential minimum, b_c and b_{NA} , and the resulting positive w_c and w_{NA} . At distances greater than 0.4 nm, the nondimensional electrostatic potential, $\bar{\phi}$, in Fig. 3(b) determines Θ_l . At $\tilde{\mu}_e = -3.4$ eV, corresponding to an electrode potential of about 0.6 V below the PZC, the surface is negatively charged and $\bar{\phi}$ is negative when $d > 0.4$ nm. Therefore, Θ_c is significantly larger than other Boltzmann factors, as shown in Fig. 3(d); this signifies the accumulation of cations in the outer Helmholtz layer at potentials below the PZC.

The last group of model parameters is determined by comparing q_{CA} calculated using Eq. (20) with those determined from the GC-DFT calculations for a range of distances d and electrode potentials [87]. These parameters are listed in Table I. Details of the GC-DFT calculations are provided in the Supplemental Material [89]. A one-to-one comparison of q_{CA} from DPFT and GC-DFT is not possible given the different charge definitions. DPFT defines q_{CA} from the projected density of states in Eq. (20), while GC-DFT uses Bader charge analysis. However, both GC-DFT and the DPFT model show two similar trends for q_{CA} , as shown in Fig. 5. On one hand, q_{CA} increases from -1 in the region of $d > 5$ Å to about -0.4 in the region of $d < 3$ Å, implying a partial charge transfer reaction from the chloride anion to Ag(111). This partial charge transfer process has been studied in detail using DFT calculations by Ávila *et al.* [62]. On the other hand, the abrupt change in GC-DFT-computed chloride charge takes place at a larger distance from the metal surface and at more negative $\tilde{\mu}_e$. The second trend means that the partial charge transfer in GC-DFT extends further in the electrolyte solution at more

positive electrode potentials. Nevertheless, the good qualitative agreement with the GC-DFT model lends credence to parameters and relationships used in the DPFT-Chem model.

IV. RESULTS

A. EDL structure

To set the stage for discussing spatially averaged quantities such as surface charge densities and differential capacitances, we first consider the spatially resolved structure of the EDL with the aid of the DPFT model. The solvent density, c_s ; cation density, c_c ; and chemisorbed anion, c_{CA} , profiles at two representative electrode potentials are shown in Figs. 6(a) and 6(c). The schematic diagrams of the EDL structures resulting from the model are depicted in Figs. 6(b) and 6(d). When drawing the schematic pictures using discrete particles, variations on the scale of 0.1 nm in the model-calculated results are filtered out. According to Eq. (16), the density profiles are determined by the Boltzmann factors, Θ_l . The discussion of Θ_l and its underlying factors in the preceding section forms the basis for understanding the density profiles and the EDL structure.

At $\tilde{\mu}_e = -4.6$ eV, corresponding to an electrode potential about 0.6 V positive of the PZC, extensive specific chemisorption of the chloride anions takes place. This is quantified by a peak in c_{CA} in the region of 0.2–0.4 nm in Fig. 6(a). This peak is accompanied by a dip in c_s , indicating replacement of the interfacial adsorbed solvent molecules by chemisorbed anions. As depicted in the corresponding schematic EDL structure in Fig. 6(b), a high concentration of chemisorbed anions and solvent molecules coexist in the region below 0.5 nm, *viz.*, in the so-called IHP. Note that the present model does not assign any specific value to the distance at which the IHP starts nor does the model require the chemisorbed anions or solvent molecules to rigidly align at the IHP, in contrast

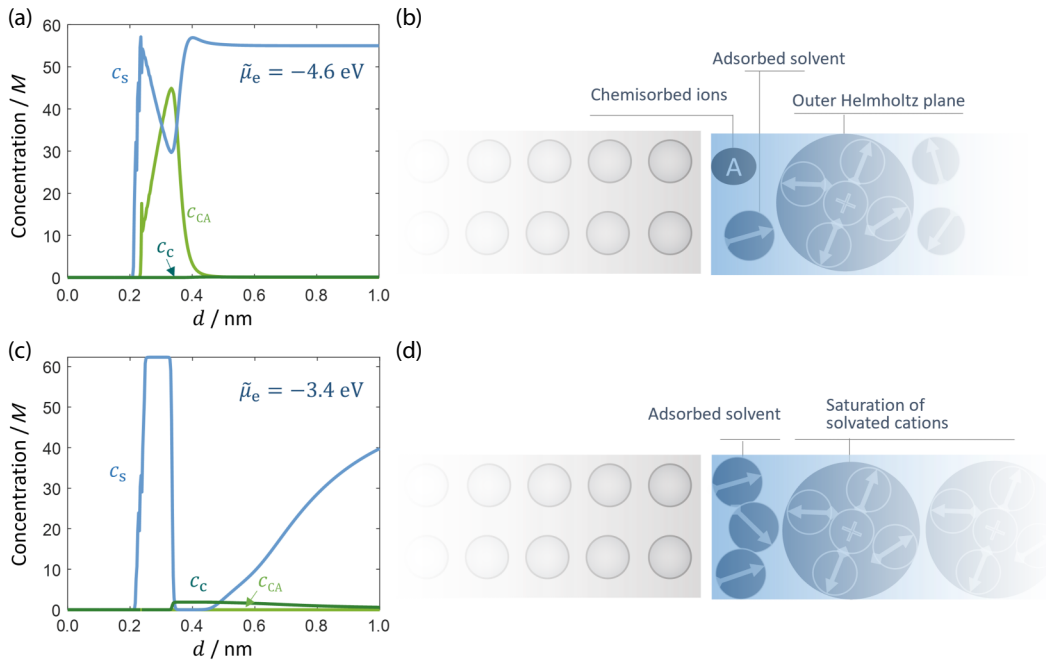


FIG. 6. Representative structures of the EDL of Ag(111) immersed in an electrolyte solution of 0.05M KPF₆ + 0.05M KCl. (a) Profiles of solvent density (c_s), cation density (c_c), and chemisorbed anions (c_{CA}) at $\tilde{\mu}_e = -4.6$ eV, and the corresponding EDL structure is pictured in (b). Results at $\tilde{\mu}_e = -3.4$ eV are displayed in (c) and (d), respectively. Density of nonspecifically adsorbing anions (not shown) depends on the electrode potential in an opposite manner compared to c_c .

to classical EDL models. Instead, the continuous density profiles are determined by the competition between the various interactions included in the Boltzmann factors of the different species. Recalling the profiles of Θ_l and its components in Fig. 3, we attribute the accumulation of chemisorbed anions in the region of 0.2–0.4 nm to the most negative w_{CA} in this region. This leads to the dominance of Θ_{CA} over those of the other components. In addition, the chemisorbed chloride anions carry a partial charge of $q_{CA} \approx -0.4$, see Fig. 5. These negatively charged chemisorbed anions attract solvated cations in the region of 0.4–0.6 nm, even though the electrode surface is positively charged, as the electrode potential is about 0.6 V positive of the original PZC. The small hump in the cation concentration, c_c , at about 0.35 nm, corresponding to an increased cation concentration, is not visible in Fig. 6(a), as the local solvent concentration, c_s , is much higher. However, this is reflected in negative σ_{free} and C_{DL} in Fig. 7.

At $\tilde{\mu}_e = -3.4$ eV, i.e., around -0.6 V below the PZC, the EDL structure is composed of a layer of adsorbed solvent molecules, c_s , around 0.2–0.3 nm, as shown in Fig. 6(c) and depicted in Fig. 6(d). This is followed by a high concentration of electrostatically bound, solvated cations, c_c , above 0.3 nm. Since the cations with a solvation shell are much larger than the solvent molecules, solvent molecules are depleted. As a result, an extended dip in the solvent concentration (c_s) is found in Fig. 6(c). The

chloride chemisorption is negligible at such a negatively charged interface.

B. Surface charge densities and differential capacitances

To study the different surface charge density and differential capacitance variants, the DPFT equations were solved for a series of $\tilde{\mu}_e$ in the range between -4.6 and -3.4 eV at 0.04 eV intervals. Figures 7(a) and 7(b) compare the experimental [65] and model-based σ_{tot} curves for Ag(111) immersed in an electrolyte solution of 0.05M KPF₆ + 0.05M KCl and 0.1M KPF₆. In addition, five surface charge densities, namely, σ_{tot} , $\sigma_{ad,tot}$, $\sigma_{ad,net}$, σ_{free} , and σ_M , were evaluated according to definitions and relationships expressed in Eqs. (3)–(7), as shown in Fig. 7(c). Three differential capacitances are derived from σ_{tot} , $\sigma_{ad,tot}$, and σ_{free} , accordingly, as shown in Fig. 7(d).

Semiquantitative agreement between the model and experiments is obtained, which is remarkable because the parameters of the EDL model were determined previously according to the experiments by Valette [106]. σ_{tot} increases as the electrode potential is made more positive. An increase in σ_{tot} corresponds to an increase in the outflow of electrons from the electrode under study to the counter electrode through the external circuit. When $-\tilde{\mu}_e < 3.8$ eV, all the surface charge densities, σ_{tot} , σ_M , and σ_{free} , are almost equal. This means that all electrons

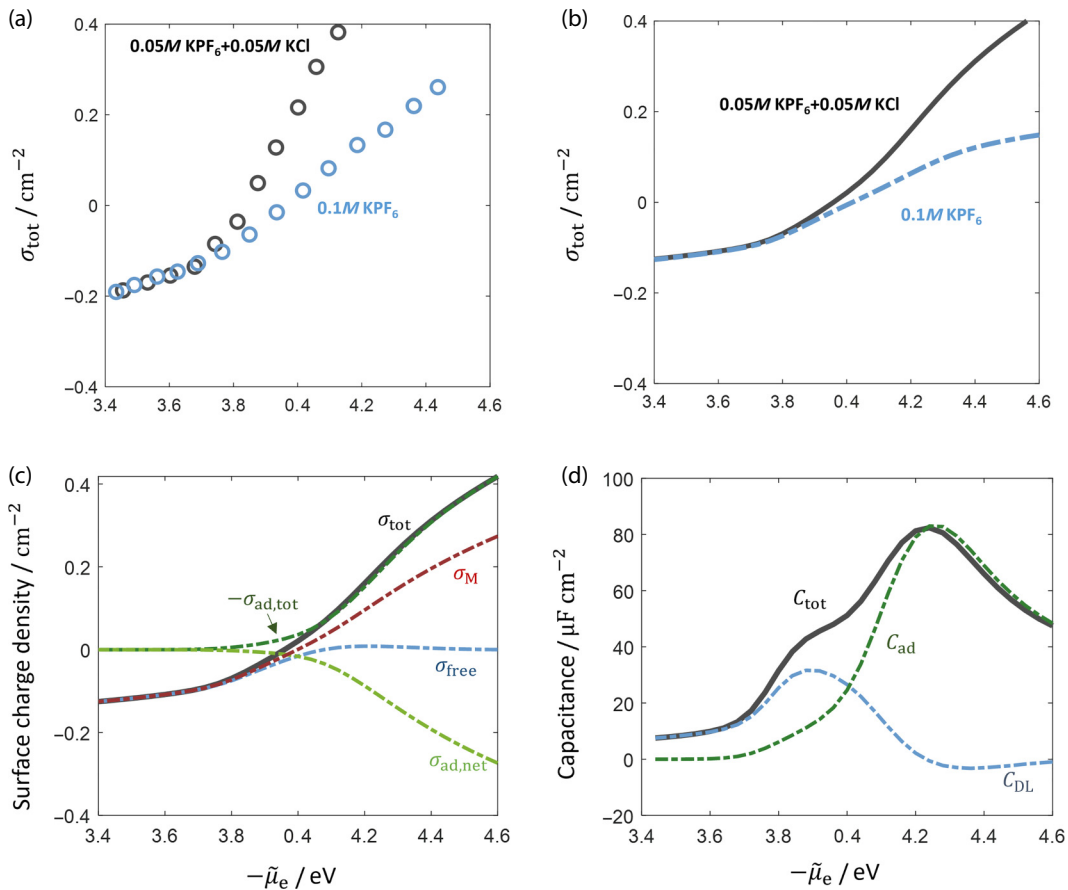


FIG. 7. (a) Experimental and (b) model-based total surface charge curves of Ag(111) immersed in an electrolyte solution of 0.05M KPF₆ + 0.05M KCl and 0.1M KPF₆. Experimental data are reproduced from Foresti *et al.* [65]. (c) Variants of surface charge densities and (d) corresponding differential capacitances of Ag(111) immersed in an electrolyte solution of 0.05M KPF₆ + 0.05M KCl. Definitions of these quantities are given in the Sec. II and the caption of Fig. 1. In calculating σ_{free} using Eq. (5), we determine the location of the OHP, according to the criterion of $w_{\text{CA}} > -1$, namely, when the short-range interaction between the metal and the anion expressed in Eq. (18) decays to the thermal energy.

entering or leaving through the circuitry are spent charging the metallic electrode, and the formation or cleavage of chemical bonds does not take place. Accordingly, at these highly negative electrode potentials, $\sigma_{\text{ad,tot}}$ and $\sigma_{\text{ad,net}}$ are zero.

Notably, the model captures the positive shift in σ_{tot} in the presence of Cl⁻ due to chemisorption when $-\tilde{\mu}_e > 3.8$ eV, corresponding to potentials more positive than -0.88 V_{SCE}. In the present model, the onset potential of chemisorption is sensitive to two parameters: the valence orbital energy, ϵ_{CA} , in Eq. (20) and the coefficient of the Morse potential, D_{CA} , in Eq. (19). At potentials higher than $-\tilde{\mu}_e = 4.0$ eV, σ_{tot} is fully determined by $-\sigma_{\text{ad,tot}}$. In other words, the free charge, $\sigma_{\text{free}} = \sigma_{\text{tot}} + \sigma_{\text{ad,tot}}$, remains almost constant and has a much smaller magnitude than σ_{tot} when $-\tilde{\mu}_e > 4.0$ eV. This implies that the electron flow is mainly caused by anion chemisorption, while the charge of the diffuse layer remains almost unchanged. A closer look

reveals that, σ_{free} decreases as $-\tilde{\mu}_e$ increases above 3.9 eV. This observation is in sharp contrast with the conventional view that σ_{free} increases monotonically with an increasing electrode potential [56]. Importantly, this unconventional surface charging behavior leads to a *negative* differential capacitance, C_{DL} , as shown in Fig. 7(d).

To understand the origin of the negative C_{DL} , we further decompose σ_{free} into contributions from the metal (σ_{M}) and the adsorbates ($\sigma_{\text{ad,net}}$), according to Eq. (7). As Fig. 7(c) shows, σ_{M} increases monotonically with increasing $-\tilde{\mu}_e$, indicating that the metallic region of the EDL becomes more positively charged, as in the traditional EDL models without chemisorption [56]. However, since the chemisorbed anions retain a fraction of their negative charge, $\sigma_{\text{ad,net}}$ becomes increasingly negative as the chloride coverage increases. When the increasingly negative $\sigma_{\text{ad,net}}$ surpasses σ_{M} , σ_{free} starts to decrease, and C_{DL} becomes negative. This $\sigma_{\text{ad,net}}$ -induced nonmonotonic

surface charging behavior has important implications for computational electrocatalysis, a point that is discussed further below.

C. Electrosorption valency

A quantitative analysis of the influence of chemisorption on the EDL structure and capacitance is obtained by studying the electrosorption valency, which was recently revisited by Hormann *et al.*, combining DFT calculations and a mean-field EDL model [39,88,108,109]. For the present case with Cl^- as the only chemisorbing species, the subscript in l_i is dropped and Eq. (11) is simplified to

$$l = -1 - \frac{1}{F} \left(\frac{\partial \sigma_{\text{free}}}{\partial \Gamma_{\text{CA}}} \right)_E, \quad (21)$$

where Γ_{CA} is the total amount of chemisorbed anions in moles per area, that is, the molar surface coverage. Equation (21) was used earlier by Garcia-Araez *et al.* in their thermodynamic analysis of C_{DL} of Pt(111) with the chemisorption of OH [110]. Note that the electrode potential, E , is fixed in the partial derivative in Eq. (21). Within our model, we can decompose the overall potential difference between the metal phase and the electrolyte phase into two parts: the potential difference between the metal phase and the IHP, $\Delta\phi^{\text{M-IHP}}$, and that between the IHP and the solution phase, $\Delta\phi^{\text{IHP-S}}$. Introducing $\Delta\phi^{\text{IHP-S}}$ as an auxiliary variable, Eq. (21) can be written as

$$\begin{aligned} l &= -1 - \frac{1}{F} \left(\frac{\partial \sigma_{\text{free}}}{\partial \Delta\phi^{\text{IHP-S}}} \right)_E \left(\frac{\partial \Delta\phi^{\text{IHP-S}}}{\partial \Gamma_{\text{CA}}} \right)_E \\ &= -1 + \frac{1}{F} C_{\text{IHP-S}}(E) \left(\frac{\partial \Delta\phi^{\text{IHP-S}}}{\partial \Gamma_{\text{CA}}} \right)_E, \end{aligned} \quad (22)$$

where $C_{\text{IHP-S}}(E) = (\partial \sigma_{\text{free}} / \partial \Delta\phi^{\text{IHP-S}})_E$ is the differential capacitance of the region confined between the IHP and the bulk solution. We use $d(\Delta\phi^{\text{IHP-S}}) = -d(\Delta\phi^{\text{M-IHP}})$ at fixed electrode potentials in the second equality. Using a capacitor model for the region between the metal surface and the IHP, $\Delta\phi^{\text{IHP-S}}$ can be approximated as the sum of an intrinsic potential difference arising from the metal electron tail, $\Delta\phi_{\text{ET}}$, and an extra potential difference due to the partially charged chemisorbates, $\Delta\phi_{\text{CA}}$,

$$\Delta\phi^{\text{IHP-S}} = \Delta\phi_{\text{ET}} + \Delta\phi_{\text{CA}} = \Delta\phi_{\text{ET}} - \frac{\Gamma_{\text{CA}} q_{\text{CA}} F \delta_{\text{IHP}}}{\epsilon_{\text{IHP}}}, \quad (23)$$

where δ_{IHP} and ϵ_{IHP} are the effective thickness and dielectric permittivity of the space between the metal surface and the IHP, respectively.

Combining Eqs. (23) and (22), the electrosorption valency can be expressed as

$$l = -1 - \frac{C_{\text{IHP-S}}}{C_{\text{M-IHP}}} q_{\text{CA}}, \quad (24)$$

where $C_{\text{M-IHP}} = \delta_{\text{IHP}} / \epsilon_{\text{IHP}}$ is the effective capacitance of the region between the metal surface and the IHP. The above analysis of the electrosorption valency is a simplified version of the more elaborate analysis conducted by Schmickler and Guidelli [64]. Nevertheless, we find that the simple expression of Eq. (24) is already very informative in grasping the potential and concentration dependency of the electrosorption valency. Our expression for the electrosorption valency in Eq. (24) shares the same idea as the expression given by Hörmann and Reuter, see Eq. (11) in Ref. [108], which involves the double layer capacitance, $C_0^{\bar{\theta}_a}$, and work function, $\Phi_0^{\bar{\theta}_a}$, at the PZC for coverage $\bar{\theta}_a$, two quantities that can be determined again from DFT calculations. On the contrary, our expression involves two modelistic capacitance components, $C_{\text{M-IHP}}$ and $C_{\text{IHP-S}}$.

In dilute solutions, the potential dependency of $C_{\text{IHP-S}}$ is more pronounced than that of $C_{\text{M-IHP}}$ and q_{CA} . Therefore, l is expected to largely follow the shape of $C_{\text{IHP-S}}$, which has a well-known camel shape with the minimum at the PZC [111]. This expectation is confirmed by the l and C_{DL} curves for 0.01M ion concentration in Figs. 8(a) and 8(b), respectively. When the ion concentration is increased to 0.1M, the PZC minimum of the l curve almost vanishes. Correspondingly, $C_{\text{IHP-S}}$ becomes smoother. Comparing Figs. 8(a) and 8(b), we find that the C_{DL} curves are largely symmetric around the PZC, but the l curves are asymmetric and exhibit much bigger peaks at more positive electrode potentials. This asymmetry is caused by both an increasing $C_{\text{IHP-S}}$ and a decreasing $C_{\text{M-IHP}}$ at more positive electrode potentials.

V. DISCUSSION

A. Implications for experimental EDLs and surface charge characterization

Experimental characterization of the local reaction conditions within the EDL is difficult because the EDL is an *interphase* [83] buried between two bulk phases. While changes in the total charge, σ_{tot} , are directly measurable, the local reaction conditions are not directly determined by σ_{tot} ; instead, the local reaction conditions depend more sensitively on the free charge, σ_{free} [26,35,36,112]. Unfortunately, σ_{free} is not directly measurable and its quantification typically requires an EDL model. In principle, the relationship in Eq. (6), $\sigma_{\text{free}} = \sigma_{\text{tot}} + \sigma_{\text{ad,tot}}$, allows one to estimate the free charge after determining $\sigma_{\text{ad,tot}}$ using thermodynamic relationships, as in Refs. [65,110,113].

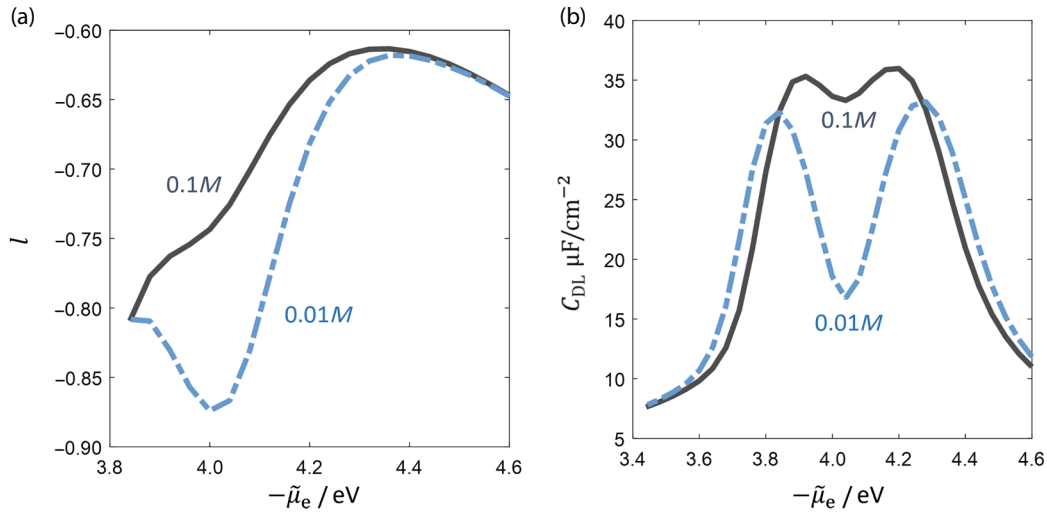


FIG. 8. (a) Electrosorption valency of chloride anion at Ag(111) immersed in an electrolyte solution of $c(1-f)M$ KPF₆ + cfM KCl. Two ion concentrations ($c=0.1$ and $0.01M$) are compared. Electrosorption valency is obtained from a linear fitting of the $\sigma_{\text{tot}} - \sigma_{\text{ad,tot}}$ relationships at five values of $f = 0, 10^{-3}, 10^{-2}, 10^{-1}$, and 0.5 ; see Fig. S1 within the Supplemental Material [89]. (b) Differential double layer capacitance curves of the Ag(111)-aqueous KPF₆ solution interface at two concentrations of 0.1 and 0.01M without chloride anions.

However, this approach suffers from low accuracy, as σ_{free} is much smaller than σ_{tot} and $\sigma_{\text{ad,tot}}$.

Another possible method is to calculate σ_{free} from C_{DL} using

$$\sigma_{\text{free}} = \sigma_{\text{free}}^{\text{ref}} + \int_{E_{\text{ref}}}^E C_{DL}^{\text{eq}}(E) dE. \quad (25)$$

It is important to note that $C_{DL}^{\text{eq}}(E)$ in this context is an equilibrium quantity [114]. In general, we can use EIS to separate $C_{DL}(E)$ from the pseudocapacitance due to chemisorption, C_{ad} , using a proper model, such as the Frumkin-Melik-Gaikazyan (FMG) model, as demonstrated in a series of works from Pajkossy *et al.* [73–77]. In extracting $C_{DL}(E)$ from experimental data using the FMG model, one needs to extrapolate to sufficiently high frequencies, where the chemisorption process does not occur due to timescale differences. Therefore, $C_{DL}(E)$ determined from EIS measurements this way is not C_{DL}^{eq} , as stressed recently [114]. Instead, it is the high-frequency component, $C_{DL,\text{HF}}$, which is characteristically different from C_{DL}^{eq} . $C_{DL,\text{HF}}$ is always positive while C_{DL}^{eq} could be negative due to the net negative charge on the chemisorbates. Negative C_{DL}^{eq} was proposed in an earlier Gouy-Chapman-Stern type model of electrocatalytic EDLs [115,116], and later confirmed by atomistic simulations [117,118]. The nonmonotonic surface charging behaviors of Pt(111)-aqueous solution interfaces due to anion chemisorption were also obtained by Zhang *et al.* using a thermodynamic analysis [113]. Wippermann *et al.* found nonmonotonic surface charging of Pt electrodes immersed in ionic liquids with a trace

amount of water [119]. Importantly, a negative C_{DL}^{eq} does not violate the stability requirement of the EDL, which is ensured by the positivity of total different capacitance, C_{tot} , in the presence of chemisorption. Interested readers are referred to a discussion on the stability of electrochemical interfaces by Partenskii and Jordan [120].

The above analysis on the difference between C_{DL}^{eq} and $C_{DL,\text{HF}}$ implies that one should not calculate σ_{free} using Eq. (25) with $C_{DL}(E)$ determined from EIS. The first method based on $\sigma_{\text{free}} = \sigma_{\text{tot}} + \sigma_{\text{ad,tot}}$ seems to be a better option. However, it is very important to gauge the errors involved in thermodynamic estimation of $\sigma_{\text{ad,tot}}$. For instance, Zhang *et al.* [113] and Garcia-Araez *et al.* [110] observed nonmonotonic behaviors in σ_{free} at Pt(111) with chemisorption of sulfate anions or OH from water dissociation. While Eq. (21) indicates that the free charge can be determined from either simulated or measured electrosorption valences, such data remains scarce. Foresti *et al.* measured the electrosorption valency of Cl⁻, Br⁻, I⁻, and S²⁻ on Ag(111) in a total concentration of 0.1M [65]. Despite the fact that the Foresti study is more than three-decades old, it constitutes the most important piece of original experimental data in recent *ab initio* thermodynamic modeling of electrosorption by Hörmann *et al.* [39, 88,108,109]. Their data show that both l_{Br} and l_{I} exhibit a “V” shape with minima obtained at around -0.8 and -1.0 V_{SCE}, respectively, which is qualitatively consistent with our results in Fig. 8. However, their work examined only a single electrolyte concentration and the concentration dependence of the l_i curve was not addressed. Hence, our observation that the l_i curve follows the C_{DL}

curve without chemisorption at more dilute concentrations remains, to the best of our knowledge, a model-based prediction.

B. Implications for electrochemical DFT simulations

The semiclassical model developed and used herein identifies an important ingredient missing from atomistic (DFT) simulation methods used for studying electrochemical interfaces: the potential-dependent chemisorbate coverage. As our results show that the varying chemisorbate coverage has a significant impact on the potential-dependent capacitance and surface charge, we argue that the common practice of fixing the surface coverage has far-reaching implications for both canonical constant-charge and semi-grand-canonical constant-potential methods. In particular, the differential capacitance used in current DFT simulations within an implicit electrolyte model is actually $C_{\text{DL,HF}}$, not $C_{\text{DL}}^{\text{eq}}$, since the relaxation of the coverage of chemisorbates is forbidden. Since $C_{\text{DL,HF}}$ and $C_{\text{DL}}^{\text{eq}}$ are characteristically different in the presence of chemisorption, see, e.g., Fig. 7, the conversion between the charge and electrode potential in current implicit electrolyte models is not fully correct. The influence of chemisorption on $C_{\text{DL}}^{\text{eq}}$ is expected to be more significant for more charged adsorbates, like the chemisorbed CO_2 ion with a net charge of around one electron on gold electrodes [29].

This is a notable deficiency because the accuracy of constant-charge and semi-grand-canonical constant-potential methods hinges on the quality of the differential capacitance used for converting between the total charge and electrode potential. As the semi-grand-canonical calculations are by design fully self-consistent, they need an accurate description of the differential capacitance *a priori* to correctly predict the total charge needed to maintain a constant electrode potential. While it is, in principle, possible to use an experimentally measured capacitance to map between the charge and electrode potential, this will impair the self-consistent nature of GC-DFT calculations. In practice, the capacitance is often calculated from an implicit electrolyte model. Therefore, if the implicit electrolyte model cannot describe chemisorption and its influence on the capacitance, the charge and number of electrons in the system at a given electrode potential will be inaccurate. For instance, a recent critical analysis on the timescales of electrochemical interfaces suggests that the EDL is in equilibrium during an electron transfer process if the activation barrier is higher than 0.3 eV [55]. This means that the local reaction conditions are determined by $C_{\text{DL}}^{\text{eq}}$, not $C_{\text{DL,HF}}$. Therefore, semi-grand-canonical simulations may wrongly describe the electrode potential and local reaction conditions in the EDL with considerably charged chemisorbates.

A similar limitation is present in canonical constant-charge calculations, even though some studies indicate that

they are more robust against inaccuracies in capacitance [51,52]. In practice, however, these canonical constant-charge calculations require mapping the surface charge to the electrode potential *via* the differential capacitance. This also raises two issues. If experimentally measured capacitances are used, the DFT calculations are no longer self-consistent or *ab initio*. Furthermore, accurate experimental capacitances are only available for a handful of surfaces, which limits the use of such constant-charge calculations.

The above discussion delineates that the accuracy and applicability of canonical and semi-grand-canonical simulations hinge on the description of the differential capacitance. Despite the promising performance of recent advances in implicit electrolyte models in DFT codes, such as the implementation of the dipolar Poisson-Boltzmann theory [121], a self-consistent and grand-canonical treatment of potential-dependent chemisorbate coverage is missing in currently available implicit continuum electrolyte models. We propose to mitigate this deficiency by augmenting the implicit solvent models with an implicit treatment of chemisorption through an Anderson-Newns model Hamiltonian. This approach achieves a good and transparent description of chemisorption-induced changes in the surface charge densities and differential capacitances. The chemisorption model can also be implemented in implicit electrolyte models available in different Kohn-Sham DFT codes with only modest efforts.

VI. CONCLUSION

We have extended the use of DPFT of EDLs to the case with chemisorption. Specifically, chemisorption is treated in an implicit manner based on the Anderson-Newns model Hamiltonian. This implicit chemisorption model has been compared with a semi-grand-canonical DFT model. Decent agreement between both models in terms of the potential and distance dependences of the partial charge number on the chloride anion adsorbed on Ag(111) has been obtained. The extended DPFT model constitutes a viable approach to model and understand the interplay between electrode charging, chemisorption, and diffuse layer charging under realistic experimental conditions. For instance, it can describe the replacement of water molecules with chemisorbed anions in the inner layer of the EDL at very positive electrode potentials.

Armed with the extended DPFT model, we have presented a detailed conceptual analysis on five variants of surface charge density and three variants of differential capacitance of electrocatalytic EDLs. We have focused on the influence of chemisorbed chloride on the free surface charge density, σ_{free} , which is not directly measurable, but which plays a crucial role in tuning the local reaction conditions within the EDL. Specifically, we have revealed that partially charged chemisorbed Cl^- possesses

a potential-dependent negative net charge density, resulting in a peculiar nonmonotonic behavior of σ_{free} : σ_{free} first increases and then decreases, as the electrode potential becomes more positive and anion chemisorption proceeds. This implies the existence of a negative differential double layer capacitance at highly positive potentials with respect to the potential of zero charge.

The influence of chemisorption on the free surface charge density has also been examined from the perspective of the electrosorption valency. A relationship between the electrosorption valency, the differential capacitances, and the partial charge number is derived. This simple relationship explains a large part of the potential and concentration dependence of the electrosorption valency. The model predicts that a dip in the electrosorption valency would appear at the PZC in more dilute concentrations.

We have also discussed the implications of our results for the experimental characterization and theoretical modeling of electrocatalytic EDLs. Regarding experimental measurements of σ_{free} , we reveal a caveat in employing EIS to determine C_{DL} and using it in the integration of C_{DL} over a range of electrode potentials to evaluate σ_{free} . The problem lies in the mismatch of frequency between C_{DL} obtained from EIS measurements and σ_{free} : while σ_{free} is an equilibrium quantity, C_{DL} extracted from EIS measurements, with the aid of a proper physical model to disentangle C_{DL} and C_{ad} , is a high-frequency nonequilibrium quantity. Therefore, we recommend determining σ_{free} from the difference between σ_{tot} and $\sigma_{\text{ad,tot}}$. However, the error involved in calculating the difference of two large surface charge densities should be carefully considered.

With regard to theoretical modeling, fixing the chemisorbate coverage in current DFT models misses out an essential feature of electrocatalytic EDLs, namely, the influence of potential-varying coverage of chemisorbates on σ_{free} and C_{DL} . Because both constant-potential and constant-charge DFT models need an accurate description of the differential capacitance, the missing contribution from the varying surface coverage negatively impacts the accuracy and generality of current DFT models of electrochemical systems. For instance, as an immediate consequence, C_{DL} obtained from such canonical or grand-canonical DFT models is always positive, and the non-monotonic surface charging behavior is totally missing. This leads to errors in the description of the local reaction conditions and the EDL. The influence of this neglect on the thermodynamics and kinetics of chemisorption and electrocatalytic reactions remains to be studied in the future. To remedy this, we propose the implicit chemisorption model as a practical and feasible approach to improve the quality of self-consistent DFT simulations of electrochemical interfaces and electrocatalytic reactions.

The data that support the findings of this study are available from the corresponding author upon reasonable request.

ACKNOWLEDGMENT

This work is supported by the Initiative and Networking Fund of the Helmholtz Association (Grant No. VH-NG-1709) and the Academy of Finland through Project No. 338228. Computational resources were provided by the CSC-IT Center for Science, Espoo, Finland.

- [1] S. Trasatti, Work function, electronegativity, and electrochemical behaviour of metals: III. Electrolytic hydrogen evolution in acid solutions, *J. Electroanal. Chem. Interfacial Electrochem.* **39** (1), 163 (1972).
- [2] J. K. Nørskov, T. Bligaard, A. Logadottir, J. R. Kitchin, J. G. Chen, S. Pandelov, and U. Stimming, Trends in the exchange current for hydrogen evolution, *J. Electrochem. Soc.* **152** (3), J23 (2005).
- [3] P. Quaino, F. Juarez, E. Santos, and W. Schmickler, Volcano plots in hydrogen electrocatalysis – uses and abuses, *Beilstein J. Nanotechnol.* **5**, 846 (2014).
- [4] A. J. Medford, A. Vojvodic, J. S. Hummelshøj, J. Voss, F. Abild-Pedersen, F. Studt, T. Bligaard, A. Nilsson, and J. K. Nørskov, From the Sabatier principle to a predictive theory of transition-metal heterogeneous catalysis, *J. Catal.* **328**, 36 (2015).
- [5] H. Ooka, J. Huang, and K. S. Exner, The Sabatier principle in electrocatalysis: Basics, limitations, and extensions, *Front. Energy Res.* **9** (2021).
- [6] T. B. Grimley, Chemisorption theory, *CRC Crit. Rev. Solid State Sci.* **6** (3), 239 (1976).
- [7] J. P. Muscat and D. M. News, Chemisorption on metals, *Prog. Surf. Sci.* **9** (1), 1 (1978).
- [8] J. K. Nørskov, Chemisorption on metal surfaces, *Rep. Prog. Phys.* **53** (10), 1253 (1990).
- [9] W. Schmickler, in *Electrochemical Science for a Sustainable Society: A Tribute to John O'M Bockris*, edited by Uosaki K. (Springer International Publishing, Cham, 2017), pp. 95–111.
- [10] T. J. Schmidt, P. N. Ross, and N. M. Markovic, Temperature dependent surface electrochemistry on Pt single crystals in alkaline electrolytes: Part 2. The hydrogen evolution/oxidation reaction, *J. Electroanal. Chem.* **524–525**, 252 (2002).
- [11] J. T. Bender, A. S. Petersen, F. C. Østergaard, M. A. Wood, S. M. J. Heffernan, D. J. Milliron, J. Rossmeisl, and J. Resasco, Understanding cation effects on the hydrogen evolution reaction, *ACS Energy Lett.* **8** (1), 657 (2023).
- [12] S. Ringe, Cation effects on electrocatalytic reduction processes at the example of the hydrogen evolution reaction, *Curr. Opin. Electrochem.* **39**, 101268 (2023).
- [13] M. F. Li, L. W. Liao, D. F. Yuan, D. Mei, and Y. X. Chen, pH effect on oxygen reduction reaction at Pt(111) electrode, *Electrochim. Acta* **110**, 780 (2013).
- [14] J. Suntivich, E. E. Perry, H. A. Gasteiger, and Y. Shao-Horn, The influence of the cation on the oxygen reduction and evolution activities of oxide surfaces in alkaline electrolyte, *Electrocatalysis* **4** (1), 49 (2013).
- [15] P. P. Lopes, D. Strmcnik, J. S. Jirkovsky, J. G. Connell, V. Stamenkovic, and N. Markovic, Double layer effects

- in electrocatalysis: The oxygen reduction reaction and ethanol oxidation reaction on Au(111), Pt(111) and Ir(111) in alkaline media containing Na and Li cations, *Catal. Today* **262**, 41 (2016).
- [16] V. Briega-Martos, E. Herrero, and J. M. Feliu, Effect of pH and water structure on the oxygen reduction reaction on platinum electrodes, *Electrochim. Acta* **241**, 497 (2017).
- [17] T. Kumeda, H. Tajiri, O. Sakata, N. Hoshi, and M. Nakamura, Effect of hydrophobic cations on the oxygen reduction reaction on single-crystal platinum electrodes, *Nat. Commun.* **9** (1), 4378 (2018).
- [18] P. Reinsberg, A.-E.-A. A. Abd-El-Latif, and H. Baltruschat, Investigation of the complex influence of divalent cations on the oxygen reduction reaction in aprotic solvents, *Electrochim. Acta* **273**, 424 (2018).
- [19] T. Kumeda, L. Laverdure, K. Honkala, M. M. Melander, and K. Sakaushi, Cations determine the mechanism and selectivity of alkaline oxygen reduction reaction on Pt(111), *Angew. Chem., Int. Ed.* **62** (51), e202312841 (2023).
- [20] A. Kozawa, Effects of anions and cations on oxygen reduction and oxygen evolution reactions on platinum electrodes, *J. Electroanal. Chem.* **8** (1), 20 (1964).
- [21] V. I. Birss and A. Damjanovic, A study of the anomalous pH dependence of the oxygen evolution reaction at platinum electrodes in acid solutions, *J. Electrochem. Soc.* **130** (8), 1694 (1983).
- [22] A. C. Garcia, T. Touzalin, C. Nieuwland, N. Perini, and M. T. M. Koper, Enhancement of oxygen evolution activity of nickel oxyhydroxide by electrolyte alkali cations, *Angew. Chem., Int. Ed.* **58** (37), 12999 (2019).
- [23] M. Görlin, J. Halldin Stenlid, S. Koroidov, H.-Y. Wang, M. Börner, M. Shipilin, A. Kalinko, V. Murzin, O. V. Safonova, M. Nachttegaal, A. Uheida, J. Dutta, M. Bauer, A. Nilsson, and O. Diaz-Morales, Key activity descriptors of nickel-iron oxygen evolution electrocatalysts in the presence of alkali metal cations, *Nat. Commun.* **11** (1), 6181 (2020).
- [24] J. Huang, M. Li, M. J. Eslamibidgoli, M. Eikerling, and A. Groß, Cation overcrowding effect on the oxygen evolution reaction, *JACS Au* **1** (10), 1752 (2021).
- [25] J. C. Fornaciari, L.-C. Weng, S. M. Alia, C. Zhan, T. A. Pham, A. T. Bell, T. Ogitsu, N. Danilovic, and A. Z. Weber, Mechanistic understanding of pH effects on the oxygen evolution reaction, *Electrochim. Acta* **405**, 139810 (2022).
- [26] S. Ringe, E. L. Clark, J. Resasco, A. Walton, B. Seger, A. T. Bell, and K. Chan, Understanding cation effects in electrochemical CO₂ reduction, *Energy Environ. Sci.* **12** (10), 3001 (2019).
- [27] T. Ludwig, J. A. Gauthier, C. F. Dickens, K. S. Brown, S. Ringe, K. Chan, and J. K. Nørskov, Atomistic insight into cation effects on binding energies in Cu-catalyzed carbon dioxide reduction, *J. Phys. Chem. C* **124** (45), 24765 (2020).
- [28] M. C. O. Monteiro, F. Dattila, B. Hagedoorn, R. García-Muelas, N. López, and M. T. M. Koper, Absence of CO₂ electroreduction on copper, gold and silver electrodes without metal cations in solution, *Nat. Catal.* **4** (8), 654 (2021).
- [29] X. Qin, H. A. Hansen, K. Honkala, and M. M. Melander, Cation-induced changes in the inner- and outer-sphere mechanisms of electrocatalytic CO₂ reduction, *Nat. Commun.* **14** (1), 7607 (2023).
- [30] A. N. Frumkin, Influence of cation adsorption on the kinetics of electrode processes, *Trans. Faraday Soc.* **55**, 156 (1959).
- [31] M. M. Waagele, C. M. Gunathunge, J. Li, and X. Li, How cations affect the electric double layer and the rates and selectivity of electrocatalytic processes, *J. Chem. Phys.* **151** (16), 160902 (2019).
- [32] N. Govindarajan, A. Xu, and K. Chan, How pH affects electrochemical processes, *Science* **375** (6579), 379 (2022).
- [33] G. Marcandalli, M. C. O. Monteiro, A. Goyal, and M. T. M. Koper, Electrolyte effects on CO₂ electrochemical reduction to CO, *Acc. Chem. Res.* **55** (14), 1900 (2022).
- [34] H. Khani, A. R. Puente Santiago, and T. He, An interfacial view of cation effects on electrocatalysis systems, *Angew. Chem., Int. Ed.* **62** (43), e202306103 (2023).
- [35] X. Zhu, J. Huang, and M. Eikerling, Electrochemical CO₂ reduction at silver from a local perspective, *ACS Catal.* **11** (23), 14521 (2021).
- [36] X. Zhu, J. Huang, and M. Eikerling, pH effects in a model electrocatalytic reaction disentangled, *JACS Au* **3** (4), 1052 (2023).
- [37] X. Zhu, J. Huang, and M. Eikerling, Hierarchical modeling of the local reaction environment in electrocatalysis, *Acc. Chem. Res.* (2024).
- [38] R. Sundararaman, W. A. Goddard, III, and T. A. Arias, Grand canonical electronic density-functional theory: Algorithms and applications to electrochemistry, *J. Chem. Phys.* **146** (11), 114104 (2017).
- [39] N. G. Hörmann, N. Marzari, and K. Reuter, Electrosorption at metal surfaces from first principles, *npj Comput. Mater.* **6** (1), 136 (2020).
- [40] M. M. Melander, Grand canonical rate theory for electrochemical and electrocatalytic systems I: General formulation and proton-coupled electron transfer reactions, *J. Electrochem. Soc.* **167** (11), 116518 (2020).
- [41] A. Bhandari, C. Peng, J. Dziedzic, L. Anton, J. R. Owen, D. Kramer, and C.-K. Skylaris, Electrochemistry from first-principles in the grand canonical ensemble, *J. Chem. Phys.* **155** (2), 024114 (2021).
- [42] A. Groß, Reversible vs standard hydrogen electrode scale in interfacial electrochemistry from a theoretician's atomistic point of view, *J. Phys. Chem. C* **126** (28), 11439 (2022).
- [43] P. Lindgren, G. Kastlunger, and A. A. Peterson, Electrochemistry from the atomic scale, in the electronically grand-canonical ensemble, *J. Chem. Phys.* **157** (18), 180902 (2022).
- [44] D. Luan and J. Xiao, Adaptive electric fields embedded electrochemical barrier calculations, *J. Phys. Chem. Lett.* **14** (3), 685 (2023).
- [45] K. Chan and J. K. Nørskov, Electrochemical barriers made simple, *J. Phys. Chem. Lett.* **6** (14), 2663 (2015).
- [46] R. Kronberg and K. Laasonen, Reconciling the experimental and computational hydrogen evolution activities of Pt(111) through DFT-based constrained MD simulations, *ACS Catal.* **11** (13), 8062 (2021).

- [47] F. Domínguez-Flores and M. M. Melander, Approximating constant potential DFT with canonical DFT and electrostatic corrections, *J. Chem. Phys.* **158** (14), 144701 (2023).
- [48] B. B. Damaskin and O. A. Petrii, Historical development of theories of the electrochemical double layer, *J. Solid State Electrochem.* **15** (7), 1317 (2011).
- [49] G. C. Gschwend and H. H. Girault, Discrete Helmholtz charge distribution at liquid-liquid interfaces: Electrocapillarity, capacitance and non-linear spectroscopy studies, *J. Electroanal. Chem.* **872**, 114240 (2020).
- [50] M. M. Melander, M. J. Kuisma, T. E. K. Christensen, and K. Honkala, Grand-canonical approach to density functional theory of electrocatalytic systems: Thermodynamics of solid-liquid interfaces at constant ion and electrode potentials, *J. Chem. Phys.* **150** (4), 041706 (2019).
- [51] S. Ringe, The importance of a charge transfer descriptor for screening potential CO₂ reduction electrocatalysts, *Nat. Commun.* **14** (1), 2598 (2023).
- [52] N. G. Hörmann, S. D. Beinlich, and K. Reuter, Converging divergent paths: Constant charge vs constant potential energetics in computational electrochemistry, *J. Phys. Chem. C* **128** (13), 5524 (2024).
- [53] G. Kastlunger, S. Vijay, X. Chen, S. Sharma, and A. Peterson, On the thermodynamic equivalence of grand canonical, infinite-size, and capacitor-based models in first-principle electrochemistry, *ChemPhysChem* e202300950 (2024).
- [54] S. D. Beinlich, G. Kastlunger, K. Reuter, and N. G. Hörmann, Controlled electrochemical barrier calculations without potential control, *J. Chem. Theory Comput.* **19** (22), 8323 (2023).
- [55] M. M. Melander, Frozen or dynamic? — An atomistic simulation perspective on the timescales of electrochemical reactions, *Electrochim. Acta* **446**, 142095 (2023).
- [56] J. Huang, Surface charging behaviors of electrocatalytic interfaces with partially charged chemisorbates, *Curr. Opin. Electrochem.* **33**, 100938 (2022).
- [57] S. Sakong and A. Groß, The electric double layer at metal-water interfaces revisited based on a charge polarization scheme, *J. Chem. Phys.* **149** (8), 084705 (2018).
- [58] J.-B. Le, Q.-Y. Fan, J.-Q. Li, and J. Cheng, Molecular origin of negative component of Helmholtz capacitance at electrified Pt(111)/water interface, *Sci. Adv.* **6** (41), eabb1219 (2020).
- [59] R. Khatib, A. Kumar, S. Sanvito, M. Sulpizi, and C. S. Cucinotta, The nanoscale structure of the Pt-water double layer under bias revealed, *Electrochim. Acta* **391**, 138875 (2021).
- [60] M. A. Gebbie, B. Liu, W. Guo, S. R. Anderson, and S. G. Johnstone, Linking electric double layer formation to electrocatalytic activity, *ACS Catal.* **13** (24), 16222 (2023).
- [61] J. Huang, Zooming into the inner Helmholtz plane of Pt(111)-aqueous solution interfaces: Chemisorbed water and partially charged ions, *JACS Au* **3** (2), 550 (2023).
- [62] M. Ávila, M. F. Juárez, and E. Santos, Role of the partial charge transfer on the chloride adlayers on Au(100), *ChemElectroChem* **7** (20), 4269 (2020).
- [63] V. Climent and J. M. Feliu, Thirty years of platinum single crystal electrochemistry, *J. Solid State Electrochem.* **15** (7), 1297 (2011).
- [64] W. Schmickler and R. Guidelli, The partial charge transfer, *Electrochim. Acta* **127**, 489 (2014).
- [65] M. L. Foresti, M. Innocenti, F. Forni, and R. Guidelli, Electrosorption valency and partial charge transfer in halide and sulfide adsorption on Ag(111), *Langmuir* **14** (24), 7008 (1998).
- [66] W. Lorenz and G. Salié, Partial charge transfer reactions in electrochemical kinetics: Review on the theory of measuring methods for electrode processes with adsorbed intermediates, *J. Electroanal. Chem. Interfacial Electrochem.* **80** (1), 1 (1977).
- [67] A. N. Frumkin and O. A. Petrii, Potentials of zero total and zero free charge of platinum group metals, *Electrochim. Acta* **20** (5), 347 (1975).
- [68] M. Wakisaka, Y. Udagawa, H. Suzuki, H. Uchida, and M. Watanabe, Structural effects on the surface oxidation processes at Pt single-crystal electrodes studied by x-ray photoelectron spectroscopy, *Energy Environ. Sci.* **4** (5), 1662 (2011).
- [69] H. S. Casalongue, S. Kaya, V. Viswanathan, D. J. Miller, D. Friebel, H. A. Hansen, J. K. Nørskov, A. Nilsson, and H. Ogasawara, Direct observation of the oxygenated species during oxygen reduction on a platinum fuel cell cathode, *Nat. Commun.* **4** (1), 2817 (2013).
- [70] J.-C. Dong, X.-G. Zhang, V. Briega-Martos, X. Jin, J. Yang, S. Chen, Z.-L. Yang, D.-Y. Wu, J. M. Feliu, C. T. Williams, Z.-Q. Tian, and J.-F. Li, *In situ* Raman spectroscopic evidence for oxygen reduction reaction intermediates at platinum single-crystal surfaces, *Nat. Energy* **4** (1), 60 (2019).
- [71] B. E. Conway and E. Gileadi, Kinetic theory of pseudocapacitance and electrode reactions at appreciable surface coverage, *Trans. Faraday Soc.* **58** (0), 2493 (1962).
- [72] V. Climent, R. Gómez, J. M. Orts, and J. M. Feliu, Thermodynamic analysis of the temperature dependence of OH adsorption on Pt(111) and Pt(100) electrodes in acidic media in the absence of specific anion adsorption, *J. Phys. Chem. B* **110** (23), 11344 (2006).
- [73] T. Pajkossy, Capacitance dispersion on solid electrodes: Anion adsorption studies on gold single crystal electrodes, *Solid State Ionics* **94** (1), 123 (1997).
- [74] T. Pajkossy and D. M. Kolb, Double layer capacitance of Pt(111) single crystal electrodes, *Electrochim. Acta* **46** (20), 3063 (2001).
- [75] T. Pajkossy and D. M. Kolb, On the origin of the double layer capacitance maximum of Pt(111) single crystal electrodes, *Electrochem. Commun.* **5** (4), 283 (2003).
- [76] T. Pajkossy and D. M. Kolb, Double layer capacitance of the platinum group metals in the double layer region, *Electrochem. Commun.* **9** (5), 1171 (2007).
- [77] T. Pajkossy, T. Wandlowski, and D. M. Kolb, Impedance aspects of anion adsorption on gold single crystal electrodes, *J. Electroanal. Chem.* **414** (2), 209 (1996).
- [78] J. Huang, Hybrid density-potential functional theory of electric double layers, *Electrochim. Acta* **389**, 138720 (2021).

- [79] J. Huang, Density-potential functional theory of electrochemical double layers: Calibration on the Ag(111)-KPF₆ system and parametric analysis, *J. Chem. Theory Comput.* **19** (3), 1003 (2023).
- [80] J. Huang, S. Chen, and M. Eikerling, Grand-canonical model of electrochemical double layers from a hybrid density-potential functional, *J. Chem. Theory Comput.* **17** (4), 2417 (2021).
- [81] J. Huang, P. Li, and S. L. Chen, Potential of zero charge and surface charging relation of metal-solution interphases from a constant-potential jellium-Poisson-Boltzmann model, *Phys. Rev. B* **101** (12), 125422 (2020).
- [82] M. M. Melander, T. Wu, T. Weckman, and K. Honkala, Constant inner potential DFT for modelling electrochemical systems under constant potential and bias, *npj Comput. Mater.* **10** (1), 5 (2024).
- [83] S. Trasatti and R. Parsons, Interphases in systems of conducting phases: Recommendations 1985 supersedes provisional version published 1983, *J. Electroanal. Chem. Interfacial Electrochem.* **205** (1), 359 (1986).
- [84] W. Mi, K. Luo, S. B. Trickey, and M. Pavanello, Orbital-free density functional theory: An attractive electronic structure method for large-scale first-principles simulations, *Chem. Rev.* **123** (21), 12039 (2023).
- [85] S. J. Sahoo, Q. Xu, X. Lei, D. Staros, G. R. Iyer, B. Rubenstein, P. Suryanarayana, and A. J. Medford, Self-consistent convolutional density functional approximations: Formulation and application to adsorption at metal surfaces, arXiv preprint [arXiv:2308.05310](https://arxiv.org/abs/2308.05310).
- [86] M. S. Shibata, Y. Morimoto, I. V. Zenyuk, and A. Z. Weber, Parameter-fitting-free continuum modeling of electric double layer in aqueous electrolyte, *J. Chem. Theory Comput.* **20** (14), 6184 (2024).
- [87] W. Tang, S. Zhao, and J. Huang, Origin of solvent dependency of potential of zero charge, *JACS Au* **3** (12), 3381 (2023).
- [88] N. G. Hörmann and K. Reuter, Thermodynamic cyclic voltammograms based on *ab initio* calculations: Ag(111) in halide-containing solutions, *J. Chem. Theory Comput.* **17** (3), 1782 (2021).
- [89] See the Supplemental Material at <http://link.aps.org/supplemental/10.1103/PRXEnergy.3.043008> for the Anderson-News Hamiltonian, details of the semi-grand-canonical first-principles calculations, tabulated adsorption grand free energy and Bader charge of a chloride anion on Ag(111), and original data for obtaining the electro-sorption valency.
- [90] A. A. Kornyshev and W. Schmickler, An Anderson model for electro-sorption, *J. Electroanal. Chem. Interfacial Electrochem.* **185** (2), 253 (1985).
- [91] W. Schmickler, A theory of adiabatic electron-transfer reactions, *J. Electroanal. Chem.* **204** (1–2), 31 (1986).
- [92] A. Held and M. Walter, Simplified continuum solvent model with a smooth cavity based on volumetric data, *J. Chem. Phys.* **141** (17), 174108 (2014).
- [93] G. Kastlunger, P. Lindgren, and A. A. Peterson, Controlled-potential simulation of elementary electrochemical reactions: Proton discharge on metal surfaces, *J. Phys. Chem. C* **122** (24), 12771 (2018).
- [94] J. P. Perdew, K. Burke, and M. Ernzerhof, Generalized gradient approximation made simple, *Phys. Rev. Lett.* **77** (18), 3865 (1996).
- [95] J. J. Mortensen, L. B. Hansen, and K. W. Jacobsen, Real-space grid implementation of the projector augmented wave method, *Phys. Rev. B* **71** (3), 035109 (2005).
- [96] A. Hjorth Larsen, *et al.*, The atomic simulation environment—a PYTHON library for working with atoms, *J. Phys.: Condens. Matter* **29** (27), 273002 (2017).
- [97] J. J. Mortensen, A. H. Larsen, M. Kuisma, A. V. Ivanov, A. Taghizadeh, A. Peterson, A. Haldar, A. O. Dohn, C. Schäfer, E. Ö. Jónsson, *et al.*, GPAW: An open Python package for electronic structure calculations, *J. Chem. Phys.* **160**, 092503 (2024).
- [98] R. Bader, *A Quantum Theory* (Clarendon, Oxford, UK, 1990).
- [99] G. Henkelman, A. Arnaldsson, and H. Jónsson, A fast and robust algorithm for Bader decomposition of charge density, *Comput. Mater. Sci.* **36** (3), 354 (2006).
- [100] F. Gossenberger, T. Roman, and A. Groß, Equilibrium coverage of halides on metal electrodes, *Surf. Sci.* **631**, 17 (2015).
- [101] A. M. Verma, L. Laverdure, M. M. Melander, and K. Honkala, Mechanistic origins of the pH dependency in Au-catalyzed glycerol electro-oxidation: Insight from first-principles calculations, *ACS Catal.* **12** (1), 662 (2022).
- [102] A. Abrashkin, D. Andelman, and H. Orland, Dipolar Poisson-Boltzmann equation: Ions and dipoles close to charge interfaces, *Phys. Rev. Lett.* **99** (7), 077801 (2007).
- [103] E. Gongadze and A. Iglič, Asymmetric size of ions and orientational ordering of water dipoles in electric double layer model - an analytical mean-field approach, *Electrochim. Acta* **178**, 541 (2015).
- [104] R. Kjellander and S. Marčelja, Correlation and image charge effects in electric double layers, *Chem. Phys. Lett.* **112** (1), 49 (1984).
- [105] D. Bratko, B. Jönsson, and H. Wennerström, Electrical double layer interactions with image charges, *Chem. Phys. Lett.* **128** (5), 449 (1986).
- [106] G. Valette, Double layer on silver single crystal electrodes in contact with electrolytes having anions which are slightly specifically adsorbed: Part III. The (111) face, *J. Electroanal. Chem. Interfacial Electrochem.* **269** (1), 191 (1989).
- [107] N. Lang, in *Theory of the Inhomogeneous Electron Gas*, edited by Lundqvist S. and March N. (Springer New York, NY, 1983), pp. 309–389.
- [108] N. G. Hörmann and K. Reuter, Thermodynamic cyclic voltammograms: Peak positions and shapes, *J. Phys.: Condens. Matter* **33** (26), 264004 (2021).
- [109] N. Bergmann, N. G. Hörmann, and K. Reuter, *Ab initio*-based modeling of thermodynamic cyclic voltammograms: A benchmark study on Ag(100) in bromide solutions, *J. Chem. Theory Comput.* **19** (23), 8815 (2023).
- [110] N. Garcia-Araez, V. Climent, E. Herrero, J. M. Feliu, and J. Lipkowski, Thermodynamic approach to the double layer capacity of a Pt(111) electrode in perchloric acid solutions, *Electrochim. Acta* **51** (18), 3787 (2006).

- [111] A. A. Kornyshev, Double-layer in ionic liquids: Paradigm change?, *J. Phys. Chem. B* **111** (20), 5545 (2007).
- [112] S. Ringe, C. G. Morales-Guio, L. D. Chen, M. Fields, T. F. Jaramillo, C. Hahn, and K. Chan, Double layer charging driven carbon dioxide adsorption limits the rate of electrochemical carbon dioxide reduction on Gold, *Nat. Commun.* **11** (1), 33 (2020).
- [113] M.-K. Zhang, J. Cai, and Y.-X. Chen, On the electrode charge at the metal/solution interface with specific adsorption, *Curr. Opin. Electrochem.* **36**, 101161 (2022).
- [114] L. Zhang and J. Huang, Measurement and interpretation of the double layer capacitance of Pt(111)/aqueous solution interfaces, *Curr. Opin. Electrochem.* **42**, 101419 (2023).
- [115] J. Huang, A. Malek, J. Zhang, and M. H. Eikerling, Non-monotonic surface charging behavior of platinum: A paradigm change, *J. Phys. Chem. C* **120** (25), 13587 (2016).
- [116] J. Huang, T. Zhou, J. Zhang, and M. Eikerling, Double layer of platinum electrodes: Non-monotonic surface charging phenomena and negative double layer capacitance, *J. Chem. Phys.* **148** (4), 044704 (2018).
- [117] R. Tesch, P. M. Kowalski, and M. H. Eikerling, Properties of the Pt(111)/electrolyte electrochemical interface studied with a hybrid DFT-solvation approach, *J. Phys.: Condens. Matter* **33** (44), 444004 (2021).
- [118] L. Braunwarth, C. Jung, and T. Jacob, Potential-dependent Pt(111)/water interface: Tackling the challenge of a consistent treatment of electrochemical interfaces, *ChemPhysChem* **24** (1), e202200336 (2023).
- [119] K. Wippermann, Y. Suo, C. Rodenbücher, C. Korte, and A. A. Kornyshev, Double layer capacitance of a platinum electrode in a protic ionic liquid: The influence of cation acidity, *Electrochim. Acta* **469**, 143207 (2023).
- [120] M. B. Partenskii and P. C. Jordan, “Squishy capacitor” model for electrical double layers and the stability of charged interfaces, *Phys. Rev. E* **80** (1), 011112 (2009).
- [121] S. M. R. Islam, F. Khezeli, S. Ringe, and C. Plaisance, An implicit electrolyte model for plane wave density functional theory exhibiting nonlinear response and a non-local cavity definition, *J. Chem. Phys.* **159** (23), 234117 (2023).